Master's Thesis 2013

Candidate: Alina Litovchenko (113912)

Title: Study on influence of geometrical features on capacity of industrial scale vertical air-lifters

Telemark University College
Faculty of Technology
Kjølnes
3914 Porsgrunn
Norway

Telemark University College
Faculty of Technology
M.Sc. Programme

MASTER'S THESIS, COURSE CODE FMH606

Student:	Alina Litovchenko		
Thesis title:	Study on influence of geometrical features on capacity of industrial scale vertical air-lifters		
Signature:	. . . . .		
Number of pages:	62		
Keywords:	vertical air-lifters predictive model		
Supervisor:	Chandana Ratnayake	sign.:	. . . . .
2nd Supervisor:	<name>	sign.:	. . . . .
Censor:	<name>	sign.:	. . . . .
External partner:	ALSTOM Power Norway	sign.:	. . . . .
Availability:	Open		

Archive approval (supervisor signature)**:** sign.: . . . . . **Date :** . . . . . .

Abstract:

The main aim of this study was to investigate the influence of operating conditions and geometrical features (fluidization air flow rate $\dot{Q}_{FA}$, transport air flow rate $\dot{Q}_{TA}$, and nozzle position z) on mass flow rate of solids in vertical air-lifters.

Results from an experimental investigation that was done with two different bulk materials have been used in the present study. The large number of experiments for small scale vertical air-lifter has been carried out at the various operating conditions.

In order to investigate wide range of experimental data and to formulate a tool for calculation of solids mass flow rate in vertical air-lifters, the mathematical model has been developed based on K – model for pneumatic conveying systems. MatLab software has been used for simulation of model and for presenting the results. Calculations have been performed by two methods: based on average and instantaneous values of pressure drop coefficient K_{st}. The first method gives a significant error and the model cannot be used for prediction of mass flow rate of solids for vertical air-lifters.

The best result was achieved based on online calculations of pressure drop coefficient and it also gave satisfactory results for predicting solids mass flow rate for different experimental conditions.

It was found that the fluidization air flow rate $\dot{Q}_{FA}$ influences most the transport capacity. Transport air flow rate $\dot{Q}_{TA}$ also influences mass flow rate of solids in vertical air-lifters. The nozzle position z has the least impact on capacity of vertical air-lifters.

Table of Contents

Preface

This is a master thesis performed at the Telemark University College in cooperation with POSTEC/Tel-Tek and ALSTOM Power Norway.

The report presents some knowledge of modeling and simulation of dynamic systems, powder technology and pneumatic conveying systems for particulate materials, and programming in MatLab.

The report consists of 7 chapters and one Appendix. First chapter introduces the theoretical background for different pneumatic conveying systems and vertical air-lifters as a subspecies of pneumatic transport. The second chapter in the thesis is dedicated to the literature review of pneumatic conveying and vertical air-lifters, different approaches for system modeling and scale up technique. Chapter three is the experimental setup. Chapter four shows the model development and explains the basis of implementation the model in MatLab. The fifth chapter discusses the results of model simulation. Chapter six is rounding of the conclusion chapter and Chapter seven gives suggestions for further work. Appendix shows the example of MatLab code for running the simulation of model.

I would like to thank my supervisor Chandana Ratnayake for help and support with the master's thesis.

Porsgrunn, June 20, 2013

Alina Litovchenko

Nomenclature

This chapter gives a list of symbols, abbreviations, and subscripts used in the thesis.

Re_{mf} – Reynolds number related to minimum fluidization velocity

Ga – Galileo number

v_{mf} – the minimum fluidization velocity, m/s

ρ_f – density of fluid, kg/m^3

η – the viscosity of the fluid, kg/ms

ρ_s – solid density, kg/m^3

g – acceleration of gravity, m/s^2

ε_{mf} – voidage at minimum fluidization

ψ –sphericity

S –constant, related to particle concentration at the onset of chocking

ε – voidage

Fr_{fd} – Froude number based on spherical particle diameter

d – spherical particle diameter, m

ε_c – voidage at chocking velocity

w_{f0} – single particle settling velocity in an unbisturbed fluid, m/s

w_b – slug velocity relative to the dense phase solids, m/s

D – tube diameter, m

Fr_{fD} – Froude number based on the tube diameter

v_ε – velocity of the porosity wave, m/s

n – function of particle Reynolds number and $({}^{d}/_{D})$ from Richardson-Zaki eguation

ΔP – pressure drop, bar

f – friction factor

ρ_a – air density, kg/m^3

v – flow mean velocity, m/s

L – length of the pipe section, m

Δp_{st} – pressure drop for the straight pipe section, bar

K_{st} – pressure drop coefficient for straight pipe section

ρ_{sus} – suspension density, kg/m^3

v_{entry} – gas velocity at the entry section of considered pipe, m/s

$\dot{m}_s$ – solid mass flow rate, kg/h

$\dot{m}_a$ – air mass flow rate, kg/h

$\dot{V}_s$ – solid volume flow rate, m^3/h

$\dot{V}_a$ – air volume flow rate, m^3/h

$\dot{Q}$ – volume flow rate of air which takes in account the compressibility effect, m^3/h

$\frac{dm}{dt}$ – change in mass in storage tank

$\dot{m}_0$ – outflow from the tank, kg/h

ε' - error in outflow to control

$\dot{m}_{0ref}$ – set point for mass flow, kg/h

m – mass flow rate, kg/h

p_{tank} – pressure in blower, bar

α – linear relationship factor for mass in blowtank related to outflow

β – linear relationship factor for blower pressure related to outflow

K – constant

L_{ev} – equivalent length of the vertical pipe section, m

L_v – length of vertical pipe section, m

$L_{b,eq}$ – equivalent length of bends, m

n – number of bends

b – bends length, m

v_a – air velocity in the considered pipe section, m/s

Δp_s – pressure drop in form of solid particle, bar

L_e – total equivalent length of the system, m

L_h–equivalent length of horizontal section of the system, m

A – pipe cross-sectional area, m^2

λ_p – non-dimensional particle pressure drop factor

$\dot{Q}_{TA}$ – transport air flow rate, m^3/h

$\dot{Q}_{FA}$ – fluidization air flow rate, m^3/h

Δz – nozzle position, m

h – length of transport pipe, m

d_p – particle diameter, m

Overview of tables and figures

This chapter shows the list of figures and tables presented in report.

1 Introduction

1.1 Overview of powder conveying technologies

Particulate solids are widely used in variety of industries, such as pharmaceutical, oil, metallurgical, paint, plastic etc. (1). Depending on production process, raw materials and finished products need to be transported within the plant and also to and/or from the plant. Different conveying technologies are used for those purposes. The most commonly applied techniques are mechanical conveyors. Few known examples for mechanical conveyors are belt, vibratory and screw conveyors. Mechanical conveying systems have number of drawbacks comparing to pneumatic transport. There are:

- Dust and fumes pollution
- Toxic dangers
- Dust explosions
- Possibility to transport only in straight line
- Required space

A simple sketch of a mechanical conveyor is shown on Figure 1-1.

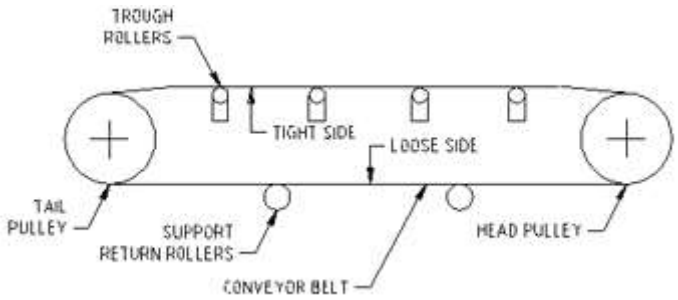

Figure 1-1: Sketch of mechanic belt conveyor (2)

Due to all those limitations and difficulties in operating of mechanical conveyors, pneumatic conveying becomes more popular in many industries.

1.2 Introduction of pneumatic

Descended from a Greek word 'pneumatikos', which means coming from the wind, pneumatic is the use of pressurized gas in various sciences and technologies.

Pneumatic conveying is one of applications of pneumatics for handling of particulate solids. This chapter tells about history, advantages and disadvantages, basic types of

pneumatic conveying systems. The motivation of this research is detail described in a later section.

1.3 Definition of pneumatic conveying

Pneumatic conveying is the transportation of wide variety of dry bulk particulate materials, both horizontally and vertically, by compressed gas stream (generally air) through pipelines. The powdered and granular solids transport by using either positive or negative pressure gradient within a piping system whereupon separate from the gas and collect at the desired place. A general scheme of a pneumatic conveying system is presented in Figure 1-2.

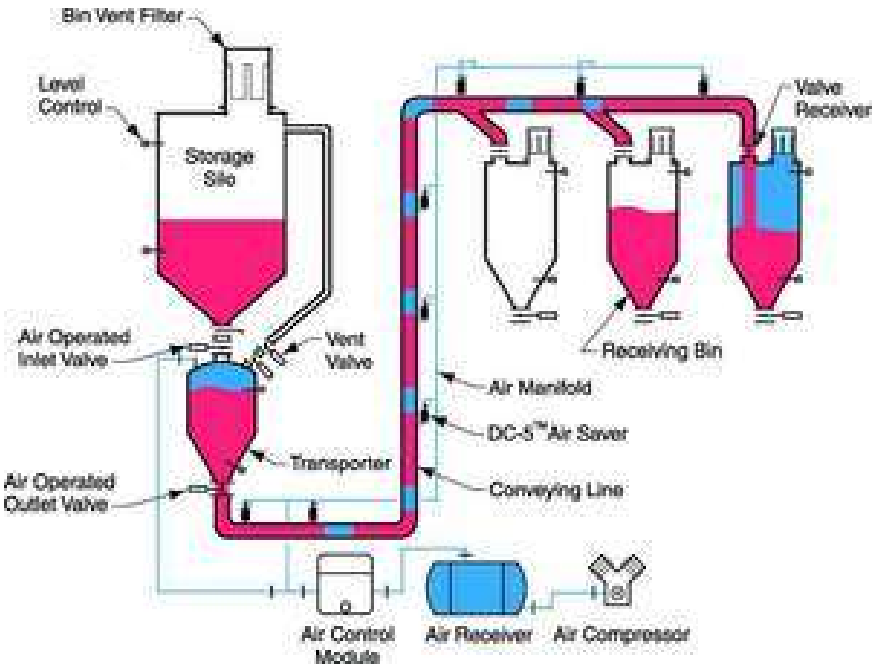

Figure 1-2: General scheme of a pneumatic conveying system (3)

The pneumatic conveying systems are applied in variety of industries, such as mining, chemical, metallurgy, food and agricultural, due to series of advantages compared to the other modes of transportation. Despite the short history of pneumatic conveyors, this mode of powder conveying has become very popular in the field of handling of bulk materials.

1.4 History of pneumatic conveying

The history of pipeline transportation starts back from antiquity. In the Roman Empire lead pipes were used for water supply and sewage disposal as well as in China

for transportation of natural gas (4). Relying on printed page references, the history of pneumatic conveying is around 150 years (5). The earliest applications to be cited are grain unloading from ships in Russia, handling of flour at a flour mill in Italy. The first pneumatic conveyor, which was recorded in 1866, ensured transportation of solid in air through the pipelined by using of fans. In last decade of 19th century the principles of pneumatic transport were widely used in Europe for transportation of grain (6). At this period of time many improvements have been done, which led to evolution of pneumatic conveying technology. Significant breakthrough in the development of pneumatic conveying can be seen during First World War due to high demand for foods, risks of explosions and labor scarceness. The very first basic studies in pneumatic conveying were done by Gasterstadt in 1923. The development of modern pneumatic conveying began in 1950's in Japan and Germany simultaneously with invention of blowers, introduction of batch conveying blow tanks etc.

Presently, pneumatic conveying is widely used for handling of particulate materials. It is reported (7) that some plants have conveying distance of more than 40 km and material flow rate of few hundred tons per hour.

1.5 Advantages and limitations of pneumatic conveying

Pneumatic conveying has a variety of applications, but it also has principal restrictions, such as material to be conveyed, distance, conveying rate, versatility, compactness, required low manpower. Total cost is also important for the selection of a conveying system. Despite of all constraints, pneumatic transport has many advantages. It offers dust-free transportation and improved working environment, reduced raw material costs, storage costs and storage area, lower production losses and saving in packing (8). Pneumatic conveying ensure flexibility in routing by adding of bends in pipelines, distribution of solids to different areas in a plant and possibility to pick–up materials from several storages (4). One of the main advantages of pneumatic transport is capability to use the same pipeline for transportation of various products including high-valued materials. Pneumatic conveyors are characterized by the efficient control and automation systems.

In spite of many factors in favor of the pneumatic transport, there are certain disadvantages, such as explosion risk, erosion, abrasion and wear due to different chemical characteristics of conveyed materials (8). Design, operate and maintain systems require special attention and high skills level due to complex flow phenomena which take place and particle degradation that may occur. Pneumatic conveying lines have limitation in distance and are high power consumers. Since pneumatic conveyors are energy-intensive it is more advisable to use them for

transportation fine particles over short distances but, as practice shows, these limitations are economic rather than technical (4).

With resent development and increase in diversity of pneumatic conveying systems, increasing in potential applications can be seen all the time.

1.6 Structure of pneumatic conveying system

Pneumatic conveying systems consist of four main zones and each of them requires special equipment to ensure the effective operation of the plant (Figure 1-3) (4). There are:

- The prime mover;
- Feeding, mixing and acceleration zone;
- The conveying zone;
- Gas-solid separation zone.

Prime mover can be represented by a fans, compressors, vacuum pumps and blowers which are used to supply gas with the amount of energy needed to convey solids.

Introduction of solid materials to the gas stream is provided in second zone by using screw feeders, venturi nozzles, rotary valves, blow vessels, etc. To move material within pipelines, particles need to pass through special designed piece of pipe in order to be accelerated.

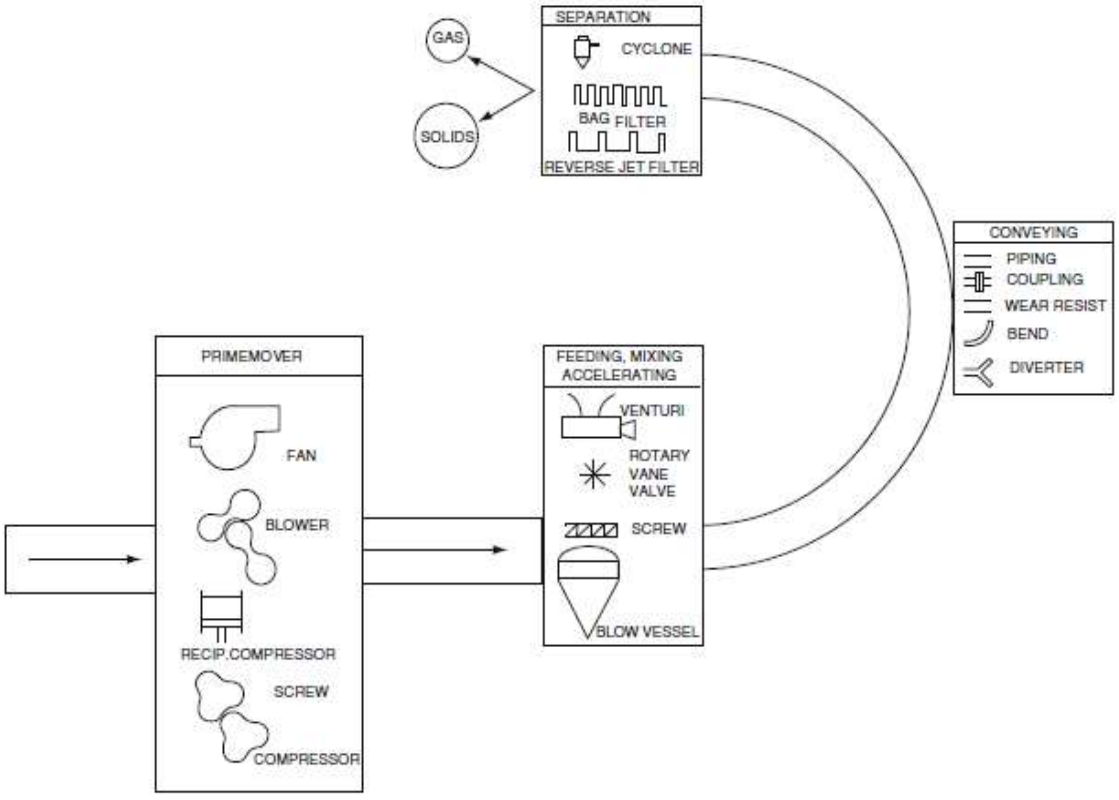

Figure 1-3: Major parts of pneumatic conveying system (4)

After passing through acceleration zone solids enter into conveying zone which consists of piping. There many factors influence on selection of pipes, such as pressure requirements, abrasiveness of material, etc.

Last zone ensure separation of particulate materials from gas. The mail factor which influences on choosing separation system is size of particles to be separated. The most often applied systems are cyclones, bag filters, reverse jet filters, etc.

1.7 Classification of pneumatic conveying systems and there modes

There are many factors and ways for classification of pneumatic conveying systems. In this subchapter, three main classifications will be considered.

Pneumatic conveying is characterized by different flow modes which depend on average concentration of particles in pipeline. Based on this, pneumatic conveying systems divided into two categories (4):

- Dilute phase regime
- Dense phase regime

Dilute phase conveying means transport of materials in suspension in the gas through the piping systems (9) as shown in Figure 1-4. This type of flow mode is the most applicable in pneumatic conveying systems.

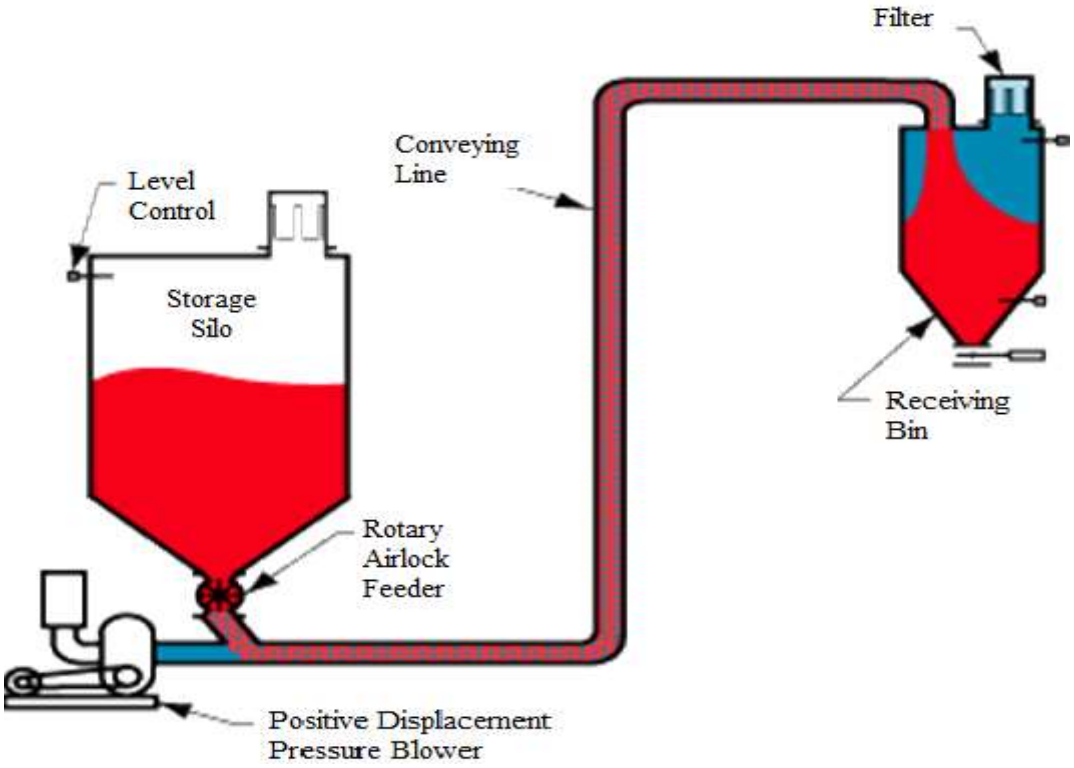

Figure 1-4: Dilute phase pneumatic conveying system (10)

Dense phase conveying takes place when solids are non-uniformly distributed over the cross-section of the pipe (4). There are several flow patterns in dense phase which can vary from the case when solids pack in pipes to the case of transportation of material as a series of dunes with a dilute phase above the dunes.

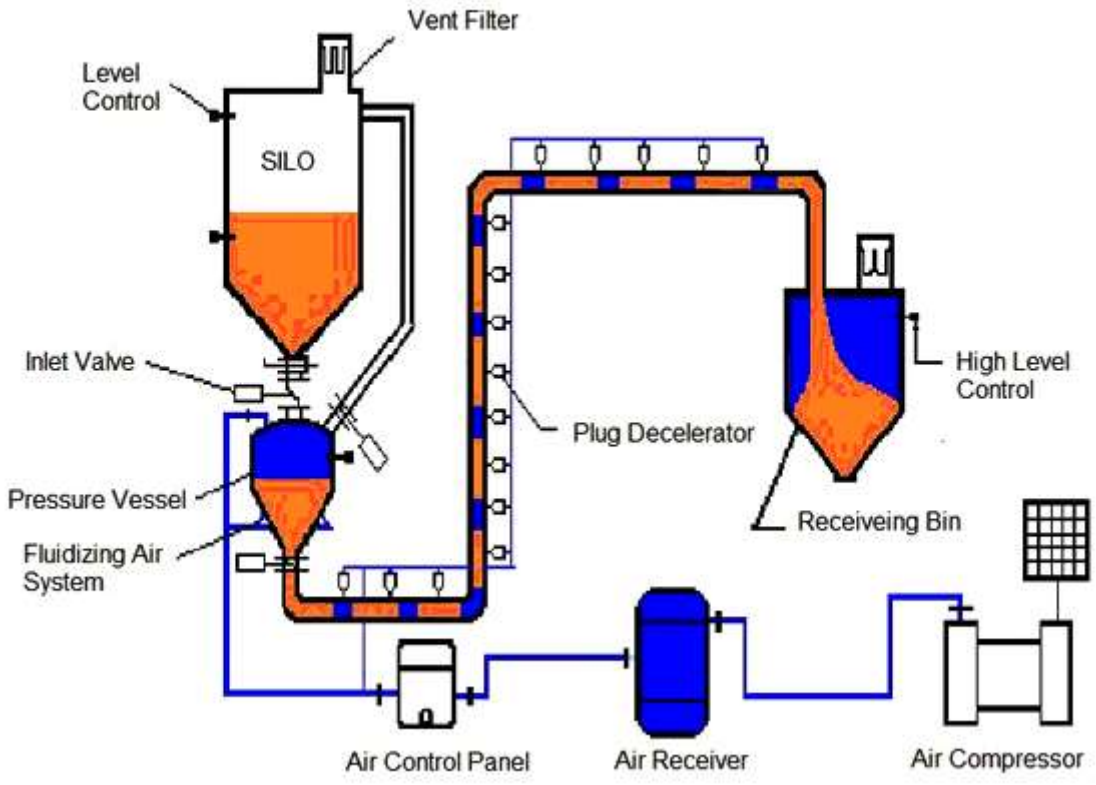

Figure 1-5: Dense phase pneumatic conveying system (11)

One of the most important factors for classifying conveying systems is operating pressure. There three main types of conveying systems based on different pressure levels (11):

1. – **Positive pressure systems** – are systems in which transportation of material and discharging to a reception point take place at atmospheric pressure. Such systems are the most widely used despite of a number of problems with feeding of solids due to a positive gas pressure in pipeline. Nowadays, there are many feeding devices that can be used in such conditions. One such positive pressure system is presented on Figure 1-6.

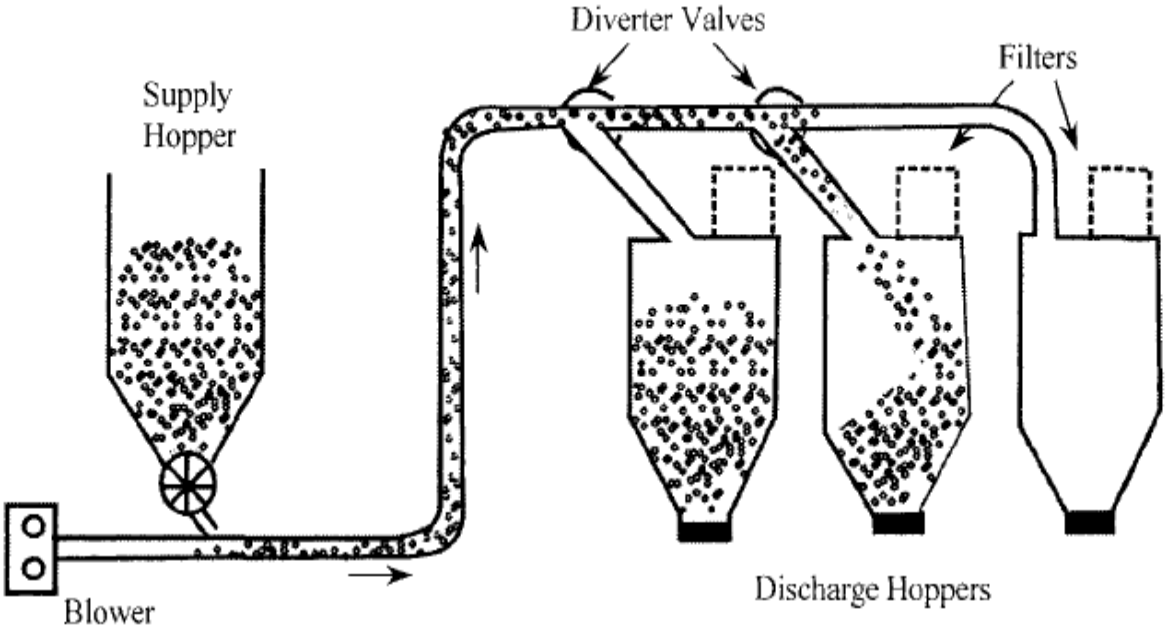

Figure 1-6: Positive pressure conveying system (9)

2. – **Negative pressure systems** – are systems with absolute gas pressure lower than atmospheric pressure (12). Those pneumatic conveying technic, which also named vacuum/suction conveying, are commonly used for transportation of solids from multiple sources to one receiving point. Also such systems are widely used for drawing of toxic and explosive materials in order to avoid all gas leakages and eliminate dust pollutions (9). Negative pressure systems can be applied for handling solids from open storage by using of suction nozzles as well as for more effective unloading ships. Typical arrangement of a negative pressure system is presented on Figure 1-7.
3. – **Combined negative-positive pressure systems** – are versatile conveying systems which combine advantages of two systems described above. Those systems, also called “suck-blow” systems, provide multiple feeding and multiple discharge of products (4). An example of combined pressure system is shown on Figure 1-8.

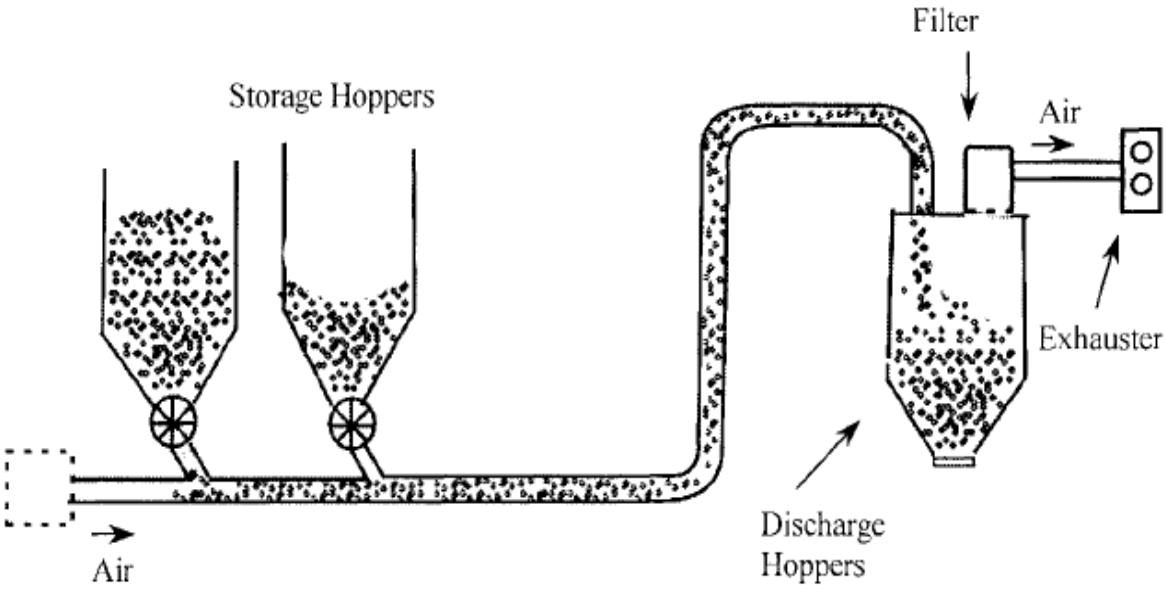

Figure 1-7: Negative pressure conveying system (9)

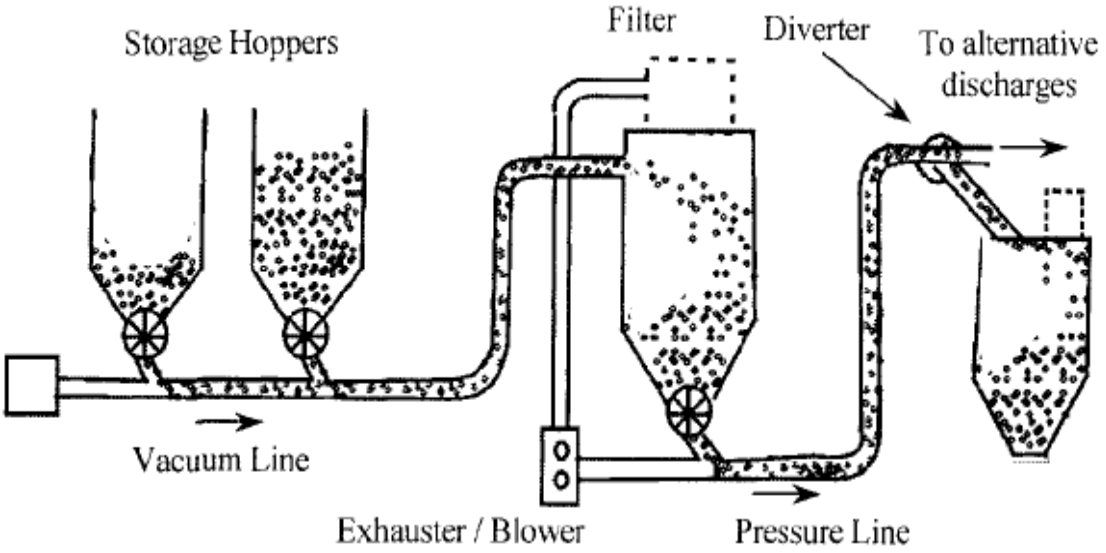

Figure 1-8: Combined negative-positive conveying system (9)

1.8 Operation of pneumatic conveying system

One of the important factors which should be taken in account in design of pneumatic conveying is distinguishable difference between flow regimes in horizontal and vertical pipes (12). The general principles of horizontal and vertical pneumatic conveying are considered further.

1.8.1 Horizontal pneumatic conveying systems

The flow regimes in horizontal conveying system can be explained by using typical phase diagram presented on Figure 1-9.

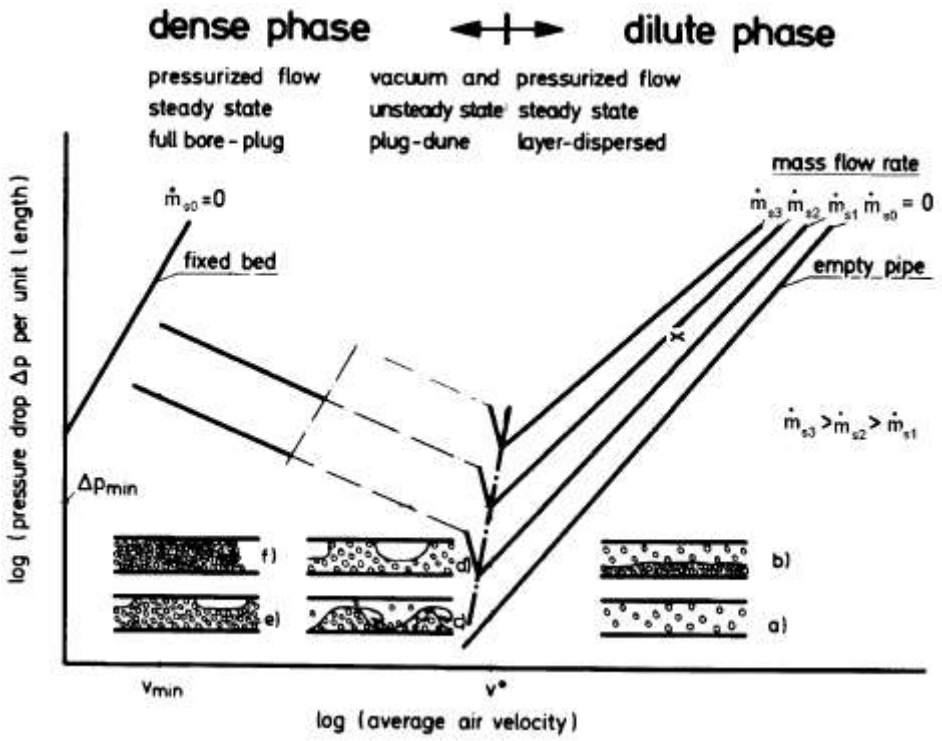

Figure 1-9: A typical phase diagram: horizontal flow (4)

The diagram shows the possible flow patterns in depending on different flow situations (12). The curves on Figure 1-9 represent different constant solids mass flow rates with the independent variation in system pressure drop and conveying gas velocity. The line M_{s0}=0 shows the case of transportation of gas only and characterize a single phase flow. Introducing of particulate material to the system leads to increasing in pressure drop compare with the case of gas only transportation. With the certain mass flow rate of particles, gas velocity is kept constant. When the gas velocity is decreasing with constant mass flow rate, reducing the pressure drop down to minimum value can be observed. The line which connects those points for different solid flow rates is pressure minimum curve. As it can be seen from the diagram, the flow regimes from the right hand side of pressure minimum curve are classified as dilute phase with the low mass loading ratios while the left hand side regimes are dense phase which characterizes by increase in pressure drop with decreasing gas velocity. This regime is unstable with plug-dune flow pattern. Further reduction of gas velocity leads to total blockage of pipeline due to the plug flow which occurs.

1.8.2 Vertical pneumatic conveying systems

As it was stated before, the position of pipes effects on pattern and characteristics of flow due to influence of gravity forces. The state diagram for vertical conveying is shown on Figure 1-10. The general shape of mass flow rate curves is similar to those for horizontal flow but the cross-sectional diagrams are totally different (12). Further discussion of vertical pneumatic conveying is presented in Chapter 2.

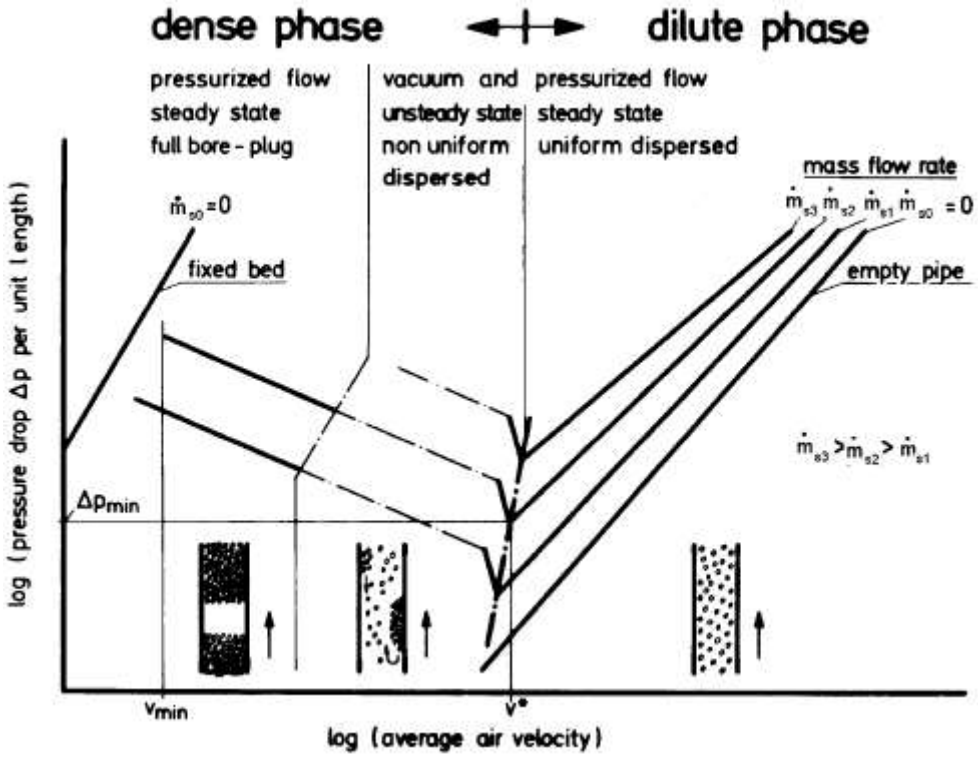

Figure 1-10: A typical phase diagram: vertical flow (4)

1.9 The aim of master's thesis

Only a few publications have looked into the factors influencing the pneumatic transport of powder materials in a vertical air-lift or similar devices. Some studies on vertical pneumatic conveyor with a fluidized bed solids feeder showed that the solids mass flow rate was dependent on a combination of transport air flow rate, fluidization air flow rate, height of the fluidized bed, and length and diameter of the transport pipe. Therefore, to develop a deeper understanding of the governing relations between the flow behaviour of gas-solids flow in a vertical lifter and its basic operating conditions geometrical features is needed for optimal operation of existing industrial scale systems and design of cost effective transport systems.

Under the present study, a detailed investigation on the process of vertical air-lifter will be carried out. The main objective of the study is to investigate the influence of

main operating conditions (fluidization air flow rate, transport air flow rate, nozzle positions, type of conveyed material, etc) of a vertical air-lifter to its transport capacity. A theoretical study based on experimental data will be planned through a scaling-up technique based on pilot scale experiments.

2 Literature Survey

2.1 Fluidization of powders

Fluidization of powder strongly depends on type of particles which make up this powder. In 1973 Geldart (13) classified particles with respect to their ability to fluidize.

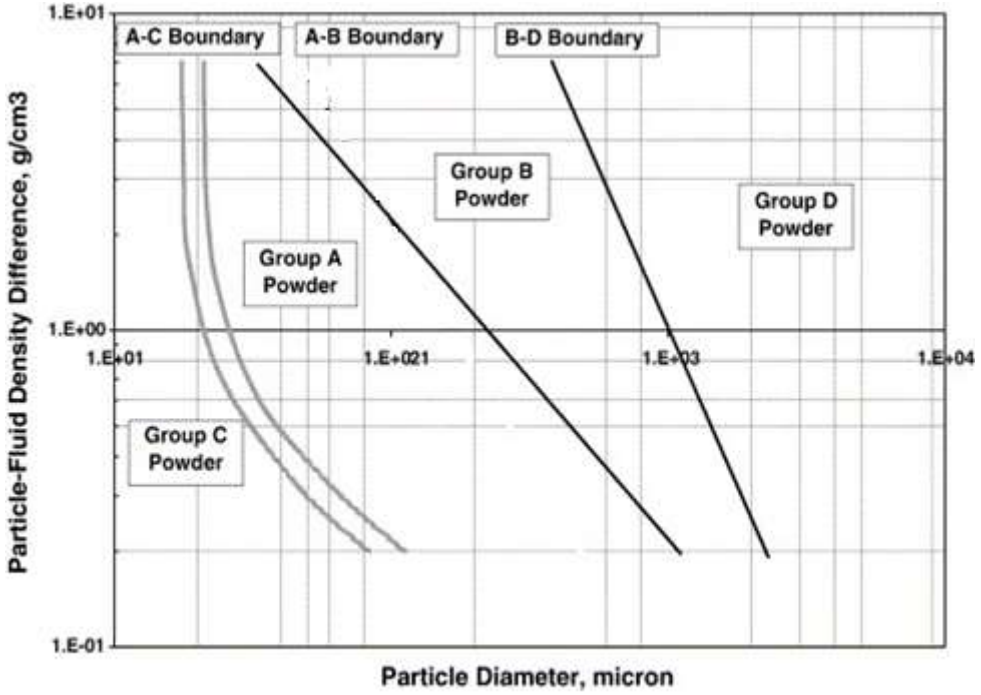

Figure 2-1: Geldart classification of particulate materials

This classification is based on the surface – volume diameter and density difference between particles and fluid (14). Geldart classified all powders into 4 groups (Figure 2-1):

- **Group A**. Powders that had been assigned to this group are aeratable and slightly cohesive. If sufficient deaeration time is not allowed between powders from group A are likely to flood. The bubbles in beds of powders rise considerably faster than the superficial air velocity. When the aeration velocity tends to zero, the collapses temporarily.
- **Group B**. These powders, which are also called sand typifies powders, are genuinely free flowing with no significant interparticulate forces. For group B is typical that the bed expansion is very small and bed collapses rapidly.
- **Group C**. Powders that are cohesive, with interparticle forces which are greater than the fluid forces. This lead to channeling in the bed. For successful

fluidization of such materials, powders must be stirred or it may be necessary to use additives.

- **Group D**. This group includes large and dense powders that have high superficial velocities at fluidization. As a result of this the segregation and attrition can be observed. A distinctive feature of this type of powders is spouting that can occur even at considerable bed depths.

Wen and Yu (15) considered the general correlation for the minimum fluidization velocity as shown below

$$Re_{mf} = (33.7 + 0.0408Ga)^{0.5} - 33.7 \qquad 2\text{-}1$$

where

$$Re_{mf} = \frac{v_{mf} x_{sv} \rho_f}{\eta} \qquad 2\text{-}2$$

$$Ga = \frac{x_{sv}^3 \rho_f (\rho_s - \rho_f) g}{\eta^2} \qquad 2\text{-}3$$

In equations above, η is the viscosity of the fluid.

$$v_{mf} = \frac{\varepsilon_{mf}^3 (\rho_s - \rho_f)(\psi x_{sv})^2 g}{150(1-\varepsilon_{mf})\eta} \qquad 2\text{-}4$$

The variety of fluidization types is shown in Figure 2-2.

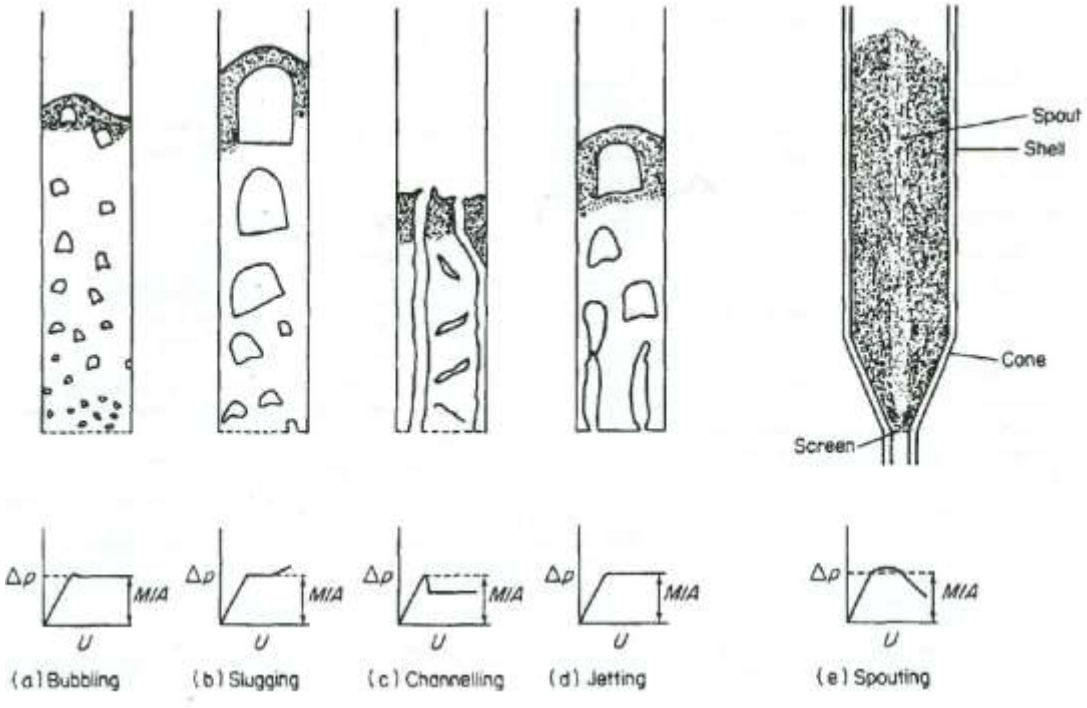

Figure 2-2: Different types of fluidization (1)

2.2 System modelling

The characteristics of vertical flow in pneumatic conveying are described quantitatively in terms of Zenz's (16). One of the most important characteristic of vertical pneumatic conveying is chocking phenomenon which has been described by Zenz and Othmer (17). The chocking point is transition point from a dilute phase vertical flow of materials to slugging or non-slugging dense phase (4). The velocity of gas at the chocking point with the particular solid flow rate is the chocking velocity. The phenomenon of chocking is not entirely investigated but there are number of different analyses on predicting of system behavior. Some of them will be considered further.

2.2.1 Analysis of Yousfi and Gau (18)

This analysis considers the stability of a uniform dilute phase flow of solids depending on a sinusoidal perturbation of gas velocity. The system becomes unstable when material concentration increases with time and distance along the riser as a result of the imposed perturbation (4). According to (18) for stable uniform dilute phase flow, a constant S is given as

$$S = \varepsilon(1-\varepsilon)Fr_{fd}^2 \qquad 2\text{-}5$$

where

$$Fr_{fd}^2 = \frac{w_{f0}^2}{gd} \qquad 2\text{-}6$$

S is related to particle concentration at the onset of chocking by

$$(1-\varepsilon_c) = \left[1-(1-\frac{4S}{Fr_{fd}^2})^{1/2}\right]^2 \qquad 2\text{-}7$$

In order to get an experimental value of S=35 the chocking voidage for polystyrene system was measured. Yousfi and Gau stated that for choking to occur

$$w_{f0}^2/gd = Fr_{fd}^2 > 4S > 140 \qquad 2\text{-}8$$

This analysis has two assumptions that change in drag force and wall effects are not accounted for. Therefore, the effect of pipe diameter on system behavior cannot be predicted.

2.2.2 Analysis of Yang (17)

In analysis by Yang (19) the stability of slugging flow is considered. It was stated that slugging conveying becomes unstable when the slug velocity w_b, relative to the dense phase solids, is higher than w_{f0}, i.e. $w_b > w_{f0}$. The slug velocity w_b is given by (20)

$$w_b = 0.35(gD)^{1/2} \quad \textit{2-9}$$

where D is the diameter of a tube. As a result, criterion by Yang can be presented as following (4)

- for no slugging

$$0.35(gD)^{1/2} > w_{f0} \quad \textit{2-10}$$

- for chocking to occur

$$w_{f0}^2/gD = Fr_{fD}^2 > 0.12 \quad \textit{2-11}$$

According to Yang analysis the key parameter to characterize the stability of the slugging conveying is Froude number based on the tube diameter.

2.2.3 Analysis of Smith (21)

Smith performed analysis of chocking and non-chocking systems based on an earlier analysis of Slis et al. (22).It was shown that the wave velocity in vertical conveyors relative to the solid velocity is the same as for a fluidized bed and can be expressed as (4)

$$v_\varepsilon = w_{f0}\varepsilon^n n(1-\varepsilon)/\varepsilon \quad \textit{2-12}$$

where

v_ε is the velocity of the porosity wave;

n is the function of particle Reynolds number and $(\frac{d}{D})$ from Richardson – Zaki equation (23).

According to Smith (21) the slug velocity is given as

$$w_b = 0.41(gD)^{0.5} \quad \textit{2-13}$$

where

D is the diameter of a tube.

Smith postulated that for chocking to occur

$$v_\varepsilon > w_b \quad \textit{2-14}$$

By combining equation it can be written as

$$\frac{w_{f0}\varepsilon^{n-1}n(1-\varepsilon)}{(gD)^{0.5}} > 0.41 \quad \textit{2-15}$$

Since ε is unknown, equation cannot be used directly. If to assume the maximum value of $\varepsilon^{n-1}(1-\varepsilon)$, the equation above can be rewritten as

$$w_{f0}n[((n-1)/n)^{n-1} - (1/n)]/(gD)^{0.5} > 0 \quad \textit{2-16}$$

Since $2.4 < n < 4.6$ (22), for $n = 2.4$ chocking will take place if

$$Fr_{fD}^2 = \frac{w_{f0}^2}{gD} > 0.59 \qquad 2\text{-}17$$

For $n = 4.6$ chocking will occur if

$$Fr_{fD}^2 = \frac{w_{f0}^2}{gD} > 0.95 \qquad 2\text{-}18$$

2.2.4 The pressure drop coefficient model

The model, also called K – model, which was developed at TEL-TEK/POSTEC by Ratnayake (12), is used for calculation of mass flow rate. Derivation of the model was made based on a model for pressure drop calculation, which was developed from Darcy's equation

$$\Delta P = 4\frac{f\rho_a v^2 L}{2D} \qquad 2\text{-}19$$

where

ΔP is the pressure drop;

f is a friction factor which is a function Reynolds number for the flow and the pipe wall roughness;

ρ_a is air density;

v is the flow mean velocity;

L is the length of the pipe section.

This model can be applied only for turbulent single phase flow. As it can be seen from equation *2-19*, pressure drop follows a square law relationship so with doubling the velocity pressure drop increases by factor of four. Since the equation of Darcy suits for single phase flow only, it was modified for two-phase flow by Ratnayake (12). Modified equation considered the two-phase flow gas-solid system as mixture with its own characteristics and different parts of piping systems separately. For the straight section of the pipe the pressure drop can be expressed as

$$\Delta p_{st} = \frac{1}{2}K_{st}\rho_{sus}v_{entry}^2\frac{\Delta L}{D} \qquad 2\text{-}20$$

where

v_{entry} is the gas velocity at the entry section of considered pipe;

K_{st} is the pressure drop coefficient for straight pipe section (horizontal or vertical);

ρ_{sus} is the density of the mixture in short pipe element.

ρ_{sus} can be calculated from the following equation

$$\rho_{sus} = \frac{\dot{m}_s + \dot{m}_a}{\dot{V}_s + \dot{V}_a} \quad 2\text{-}21$$

where

$\dot{m}_s$ and $\dot{m}_a$ are the solid and air mass flow rate respectively;

$\dot{V}_s$ and $\dot{V}_a$ are solid and air volume flow rate respectively.

The mass flow rate can be expressed by re-arranging equation *2-21*

$$\dot{m}_s = \frac{\rho_a \dot{Q} - \rho_{sus} \dot{V}_a}{\frac{\rho_{sus}}{\rho_a} - 1} \quad 2\text{-}22$$

where

$\dot{Q}$ is the volume flow rate of air including the experimentally measured air volume flow rate at the true pressure in the section of the pipeline that is considered. This is takes into account the compressibility effect.

2.3 Control of pneumatic conveying systems

Control systems for pneumatic conveying were considered by Klinzing et al (4). This chapter describes the modeling of a positive pressure blowtank system for application of PID-control.

Modeling of the system, mentioned above, can be done as mass balance with an assumption that the output from the tank can be measured.

$$\frac{dm}{dt} = -\dot{m}_0 \quad 2\text{-}23$$

where

$\frac{dm}{dt}$ – change in mass in storage tank

$\dot{m}_0$ – outflow from the tank

By specifying a set point for mass outflow of materials from the tank, the error to control is determined by equation:

$$\varepsilon' = \dot{m}_{0ref} - \dot{m}_0 \quad 2\text{-}24$$

where

ε' – error in outflow to control

$\dot{m}_{0ref}$ – set point for mass flow

$\dot{m}_0$ – measured outflow from the tank

The output can be determined as a function of blowtank pressure and mass of solids in the tank with assuming a linear dependence between those variables. According to Klinzing et al (4) the model for mass flow out of tank is as follows:

$$\dot{m}_0 = \alpha m + \beta p_{tank} \quad 2\text{-}25$$

where

p_{tank} – pressure in blower

β – linear relationship factor for blower pressure related to outflow

α – linear relationship factor for mass in blowtank related to outflow

$$p_{tank} = K \cdot \varepsilon' \quad 2\text{-}26$$

$$p_{tank} = K(m_{0ref} - m_0) \quad 2\text{-}27$$

Final model for outflow of the tank is written by combining equation:

$$\frac{dm}{dt} = -\dot{m}_0 \quad 2\text{-}28$$

$$\frac{dm}{dt} = -(\alpha m + \beta p_{tank}) \quad 2\text{-}29$$

$$\frac{dm}{dt} = -[\alpha m + \beta K(\dot{m}_{0ref} - \dot{m}_0)] \quad 2\text{-}30$$

In order to get transfer function for model above, the Laplace transform was applied:

$$\frac{dm}{dt} + \alpha m = -\beta K(\dot{m}_{0ref} - \dot{m}_0) \quad 2\text{-}31$$

$$sm(s) + \alpha m(s) + m(0) = -\beta K(\dot{m}_{0ref}(s) - \dot{m}_0(s)) \quad 2\text{-}32$$

$$m(s) = \frac{1}{s+\alpha}[m(0) - \beta K\left(m_{0ref}(s) - m_0(s)\right)] \quad 2\text{-}33$$

where

$m(0)$ – the initial mass in blowtank

The transfer function is like in equation

$$m(s) = e^{-\tau s}\frac{1}{s+\alpha}[m(0) - \beta K\left(m_{0ref}(s) - m_0(s)\right)] \quad 2\text{-}34$$

where

$e^{-\tau s}$ – transport delay

This transfer function can be controlled by PID-control system but in order to avoid oscillations due to noise PI-controller should be used. As alternative option Klinzing et al (4) suggests modeling by neural networks and control by fuzzy logic.

2.4 Scale up techniques

Some methods that are used for modeling and predicting of different characteristics of pneumatic conveyors involve experiments in a pilot scale rig over a wide range of operating conditions. The obtained data need to be scaled by experimentally determined factors to be used for modeling and predicting full scale system behavior (12).

The scaling of experimental data is one of the most important stages of the design of pneumatic conveying systems since it gives a link between pilot scale apparatus and industrial full- scale rigs. Therefore, it has essential accuracy and reliability.

In general, there are two approaches in scaling up techniques presented in literature. There are global testing approach and the piecewise approach (12). Both of them have advantages and disadvantages.

2.4.1 Mills scaling technique

Mills (24) considered that conveying conditions are the same for the laboratory-scale rig and full-scale installation. The scaling procedure is to carry out in two stages:

- Scaling to the required distance with considering vertical sections and bends;
- Scales the characteristics of conveying process in terms of the pipe diameter.

In order to compensate different effects of bends in pilot plant and industrial apparatus the concept of equivalent length of a bend has been introduced (12).

2.4.1.1 Effect of direction

For the horizontal pipe section experimental data from pilot rig contribute directly to the equivalent length of the full-scale installation, by reason of the same magnitude as its physical length.

The vertical section is considered to be scaled with parameters in terms of length of straight horizontal pipe. Since the pressure drop in vertical pipe line is twice higher that in horizontal section, the equivalent length of for the vertical pipe section can be expressed as

$$L_{ev} = 2L_v \qquad 2\text{-}35$$

2.4.1.2 Effect of bends

The same principle can be applied for equivalent length of bends but, since it's not an independent parameter , the variation of bend's length in terms of the conveying material needs to be found by using pilot plant (12).

$$L_{b,eq} = nb \qquad 2\text{-}36$$

2.4.1.3 Length of whole system

The total equivalent length can be calculated by using a reciprocal law $m_s \propto (\frac{1}{L_e})$ for a constant Δp_s and v_a. That is, $m_{s2} = m_{s1}(\frac{L_{e1}}{L_{e2}})$. Where, for a constant Δp_s and v_a, the total length can be expressed as

$$L_e = L_h + L_{ev} + L_{eb} \quad \textit{2-37}$$

2.4.1.4 Pipe diameter

The scaling up technique which is suggested by Mills (24) is based on pipe cross – sectional area $m_s \propto A \propto D^2$ for a constant $m_a D^{-2}$ and Δp_s. Also m_s can be considered in terms of pipe diameter as it presented below

$$m_{s2} = m_{s1}(\frac{D_2}{D_1})^2 \quad \textit{2-38}$$

and

$$m_{a2} = m_{a1}(\frac{D_2}{D_1})^2 \quad \textit{2-39}$$

For determination of the minimum conveying limits Mills (24) suggested to use 'trial and error' procedure, since the most important parameters of conveying system are interrelated.

2.4.2 Wypych and Arnold scaling method

Mills (24) scale up method has been tested by Wypych and Arnold (25) and it was concluded that the equation used in Mills technique are not valid, especially when data are scaled-up with respect to diameter of pipes (12). The following scale-up equation was suggested

$$m_{s2} = m_{s1}\frac{L_1'}{L_2'}(\frac{D_2}{D_1})^{2.8} \quad \textit{2-40}$$

where

L_1' and L_2' are the adjusted values of length that represent differences between the number and type of bends in the laboratory rig and full – scale plant.

This research doesn't include the effects of bends in pipeline and no allowance has been made for the bends when total length is calculated (12).

2.4.3 Molerus scaling technique

Technique presented in (26) considers non-dimensional parameters as it shown below:

$$\lambda_p \equiv \frac{2\left(\Delta p_s/\Delta L\right)D}{\mu \rho_a v_a^2} \quad \textit{2-41}$$

$$Fr_a \equiv \frac{v_a}{\sqrt{Dg}} \quad \textit{2-42}$$

where

λ_p is non-dimensional particle pressure drop;

Δp_s is the pressure drop in form of solid particle (12).

Molerus (26) determined that the combination of these two parameters describes fully suspended gas-solid flow for given combination of gas and conveyed material. According to this method, pilot plant tests are carried out to get the data in terms of $\lambda_p$vs. Fr_a and to use the resulting curve for the prediction of the pressure drop of the plant to be designed (12).

2.5 Vertical air-lifters

The least studied type of pneumatic transport is the vertical air-lifters since only a several publications have investigated the factors influencing the transport of solids in these devices. As presented in some references ((28) and (29)), solids mass flow rate in vertical pneumatic conveyors with fluidized bed solids feeder depends on transport air velocity rate, fluidization air flow rate, height of the fluidized bed, length and diameter of pipe (30). Latter work primarily focused on measuring particle velocity in pipe cross – section by using laser Doppler anemometry (31). As anticipated, the particle velocity increases with increasing superficial air velocity and decreasing particle size and density (30). It was stated by Marthiesen and Solberg (31) that the distance z between the nozzle outlet and the transport pipe inlet also influence on mass flow rate of materials and with increasing distance z at a constant transport air flow rate, increasing in mass flow rate of solids can be observed.

The flow behavior in pneumatic transport can be described by using flow diagrams. There are two main flow regimes which can occur: dilute and dense phase. In order to avoid unstable conditions in dense phase and unnecessarily high pressure in dilute phase Raczek et al. (32) suggests to carry out vertical pneumatic conveying systems in dilute phase near the point of the minimum pressure drop. The minimum pressure drop depends on particle properties, characteristics of the system and operating conditions, however, no study on vertical air-lifts performed to characterize the relationship between main system parameters, such as the transport air velocity, mass flow rate of materials and the pressure drop (30) .

3 Experiment

3.1 Experimental rig

For developing a mathematical model for predicting solids mass flow rate, it was decided to use the data from a previous experiment, which has been carried out at POSTEC by Jana Chladek (30). Experiment was carried out in a 4 m high vertical air-lifter that is presented on Figure 3-1.

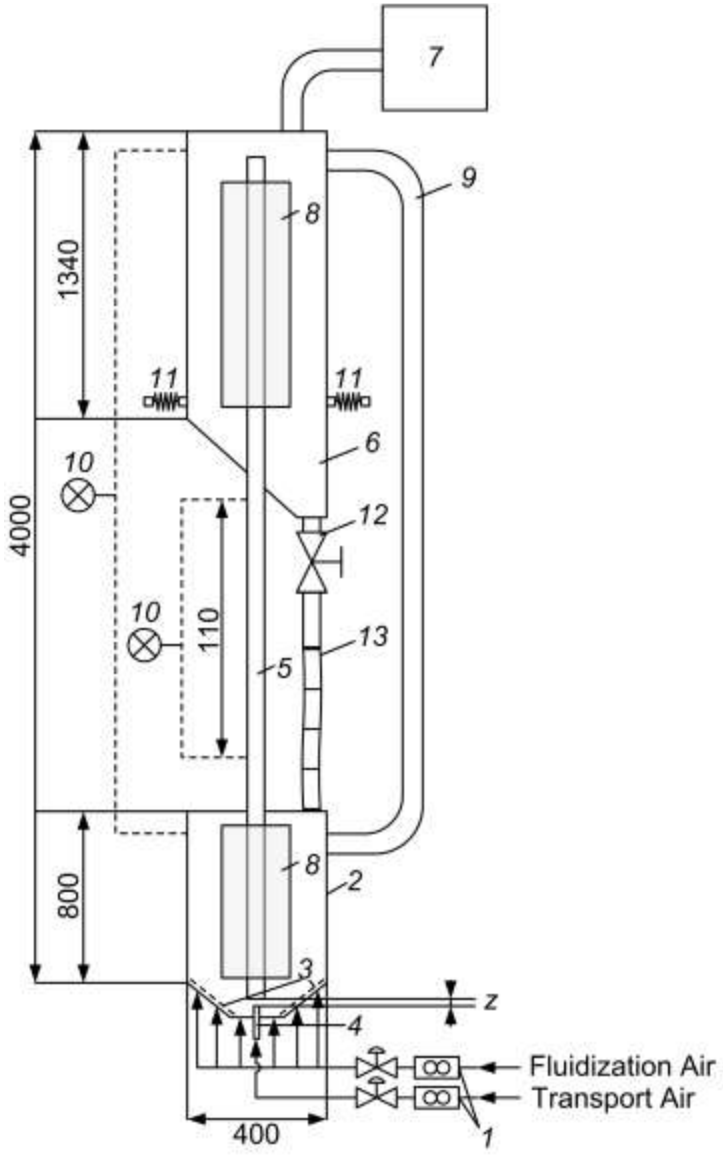

Figure 3-1: Schematic diagram of the experimental rig

For measuring the fluidization air flow rate and transport air flow rate was installed flow meter 1. In order to have uniform fluidization of the solids, the fluidization air was supplied to the bottom of the feed tank 2 through an air distribution plate 3 (air permeable fabric) in several positions. The transport air supplied to the feed tank by a cylindrical steel nozzle 4 with the internal diameter of 15 mm. The nozzle position can

vary, however, in this experiment, the distance between nozzle outlet and transport pipe inlet was 2 cm and 3 cm (i.e., $z = 2$ cm, $z = 3$ cm). The transport pipe 5 with internal diameter of 42 mm was made of steel. The transport air moved the conveyed material through the transport pipe to the receiving tank 6, which was ventilated to the atmosphere. For collecting escaping particles from the conveying air the paper bag filter 7 was installed at the air exhaust. Glass windows 8 provided the possibility of easy inspection. The feed and the receiving tank were connected with the bleed line 9 with internal diameter of 80 mm to avoid any pressure build-up between the tanks. The differential pressure transmitter 10 (0-100 mbar, EJX110A, Yokogawa) was used for monitoring the pressure difference between the feed and the receiving tank. Another differential pressure transmitter 10 (0-100 mbar, EJX110A, Yokogawa) was measuring the pressure drop along the transport pipe. This transmitter was connected to two pressure taps positioned approximately 1,15 and 2,25 m above the transport pipe inlet. In order to evaluate the mass flow rate of material during the conveying, three load cells 11 (Z6FC3, HBM) were installed on the receiving tank. The differential pressure transmitters and the load cells were connected to a data acquisition card (NI9239, National Instruments). All experimental data was recorded on a PC running LabVIEW 8.5 (National Instruments). During the experiment the valve 12 on the return line 13 was closed. At the end of an experiment, the valve was opened to discharge the receiving tank.

3.2 Operating conditions

The experiment was carried out for two types of material: glass beads and zirconium oxide. Properties for these solids presented in Table 3-1.

Table 3-1: Material properties (30).

Material	Particle size (μm)	Average particle diameter (μm)[a]	Particle density (kg/m^3)	Particle terminal velocity (m/s)	Minimum fluidization velocity (m/s)
Glass beads	100-200	150	2500	0.9	0.019
Zirconium oxide	200-300	260	3800	2.3	0.102

During the experiments the variation of transport air flow rate and fluidization air flow rate was ensured in order to study their influence on solids mass flow rate in vertical air-lifters. The transport air flow rate varied from 24 to 100 Nm^3/h, that corresponds to the superficial air velocity of 5 to 21 m/s, respectively, with

assumption that all the air passing through the nozzle enters the transport pipe. The fluidization air flow rate ranged from 0-12 Nm^3/h for glass beads and 0-60 Nm^3/h for zirconium oxide.

4 Mathematical model

The mathematical model that can be used to predict solids mass flow rate for various nozzle positions, transport air flow rate, fluidization air flow rate and particle size was developed based on K-model (12). Generally model looks like

$$\dot{m}_s = f(\dot{Q}_{TA}, \dot{Q}_{FA}, \Delta z, d_p) \qquad 4\text{-}1$$

where, $\dot{Q}_{TA}$ is transport air flow rate, m³/h;

$\dot{Q}_{FA}$ is fluidization air flow rate, m³/h;

Δz is a nozzle position, m;

d_p is the particle diameter, m.

From the Equation 2-20

$$\Delta p_{st} = \frac{1}{2} K_{st} \rho_{sus} v_{entry}^2 \frac{\Delta L}{D}$$

Assume velocity of fluidized material is approximately equal to the velocity of single particle

$$v_{entry} = v_p = \frac{\dot{Q}_{TA}}{A} = \frac{4\dot{Q}_{TA}}{\pi d_p^2} \qquad 4\text{-}2$$

$$\Delta p_{st} = \frac{1}{2} K_{st} \rho_{sus} \left(\frac{\dot{Q}_{TA}}{A}\right)^2 \frac{h + \Delta z}{D} =$$

$$\frac{1}{2} K_{st} \rho_{sus} \left(\frac{4\dot{Q}_{TA}}{\pi d_p^2}\right)^2 \frac{h + \Delta z}{D} =$$

$$8 K_{st} \rho_{sus} \left(\frac{Q_{TA}}{\pi d_p^2}\right)^2 \frac{h+\Delta z}{D} \qquad 4\text{-}3$$

$$\rho_{sus} = \frac{\Delta p_{st}}{8 K_{st} \left(\frac{\dot{Q}_{TA}}{\pi d_p^2}\right)^2 \frac{h+\Delta z}{D}} \qquad 4\text{-}4$$

After inserting Equation 4-3 into Equation 2-22

$$\dot{m}_s = \frac{\rho_a \dot{Q}_{FA} - \frac{\Delta p_{st} \pi^2 d_p^4 D}{8 K_{st} \dot{Q}_{TA}^2 (h+\Delta z)} \dot{Q}_{TA}}{\frac{\Delta p_{st} \pi^2 d_p^4 D}{8 K_{st} \dot{Q}_{TA}^2 (h+\Delta z) \rho_a} - 1} \qquad 4\text{-}5$$

To be able to use Equation 4-5, pressure drop coefficient needs to be calculated. It can be done by using the following equation

$$K_{st} = \frac{\Delta p_{st}}{8 \rho_{sus} \frac{\dot{Q}_{TA}^2}{\pi^2 D^4}} \qquad 4\text{-}6$$

The model above was implemented in MatLab by using simple *for* – loop. The example of MatLab script is presented in Appendix 1. For running the model, input

data were imported from Excel file by using special MatLab commands such as *xlsread*. It makes possible to run the script for different sets of input data from different Excel files.

5 Results and discussion

This chapter represents the results of model prediction for different experimental conditions and comparing calculated and measured data for various experiments. Calculations were carried out by two methods: based on instantaneous data and based on average data.

5.1 Instantaneous data: zirconium oxide

The following subchapter shows the results of model simulation for experiment with zirconium oxide based on instantaneous data.

Pressure drop coefficient calculated for 100FA 20TA and nozzle position 2 cm is shown on Figure 5-1.

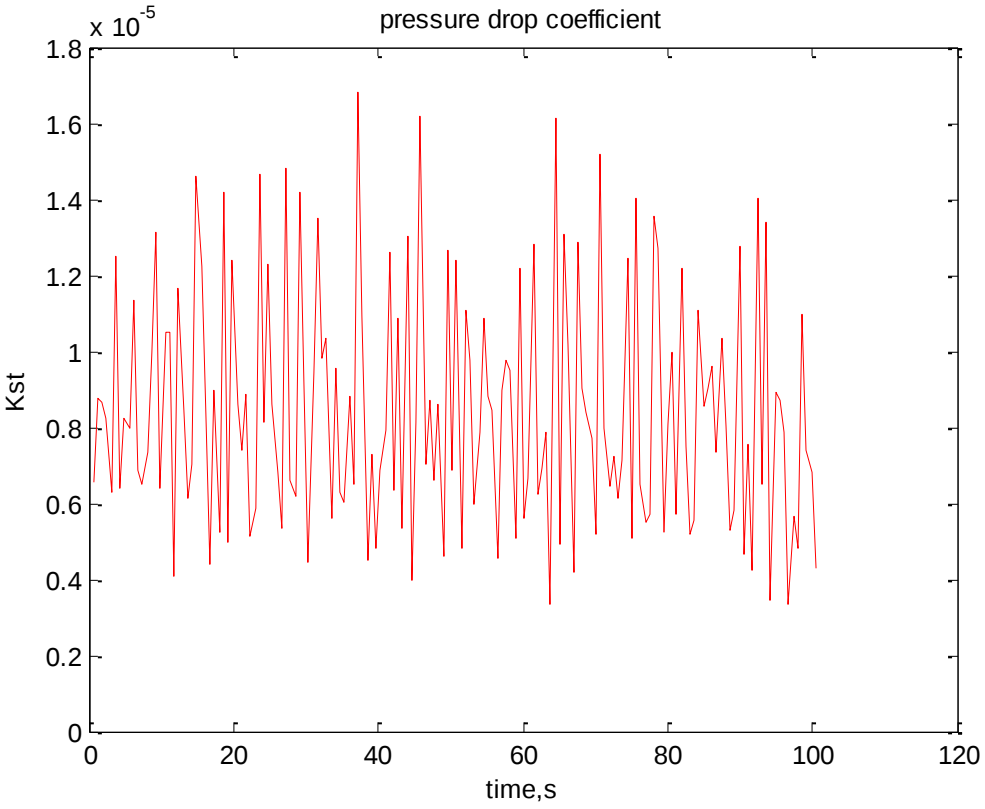

Figure 5-1: Pressure drop coefficient for 100FA 20TA 2cm experiment with zirconium oxide

As it can be seen from the graph pressure drop coefficient varies with time. In order to calculate solids mass flow rate for this experiment, calculated pressure drop coefficient for each moment of time was inserted in model for mass flow rate. The results of these calculations presented on Figure 5-2.

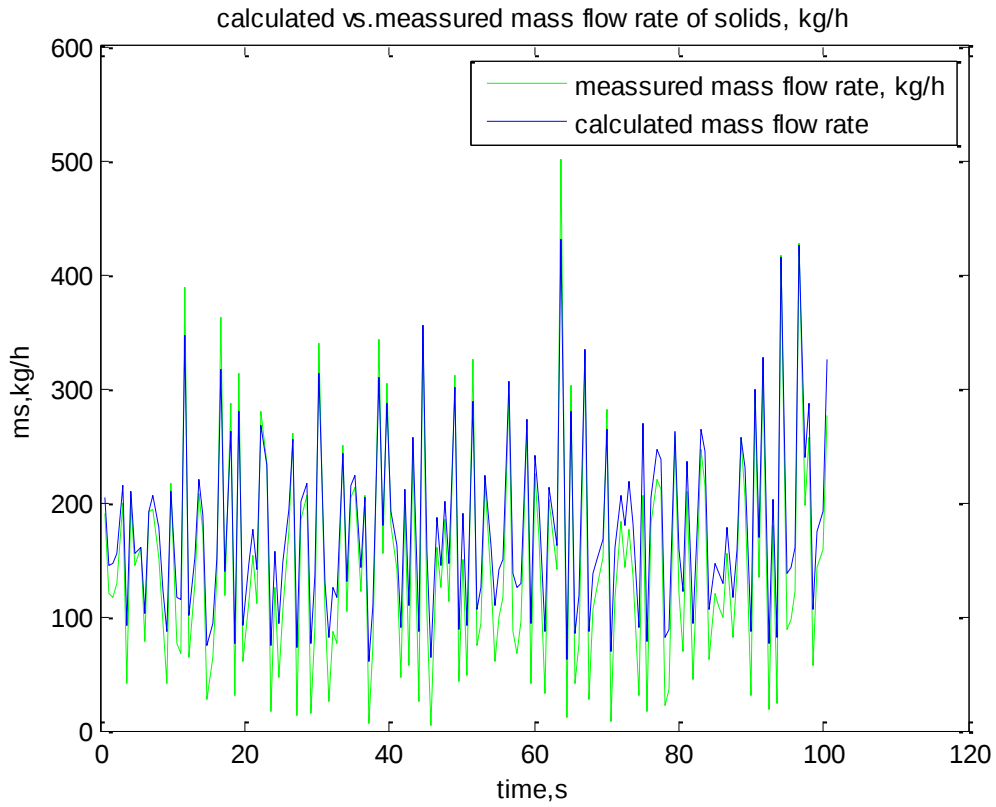

Figure 5-2: Calculated vs. measured mass flow rate for 100FA 20TA 2cm experiment with zirconium oxide

Figure 5-2 shows calculated and measured mass flow rate of zirconium oxide for the experiment with fluidized air flow rate $\dot{Q}_{FA} = 100\ {}^{m^3}/_{h}$, transport air flow rate $\dot{Q}_{TA} = 20\ {}^{m^3}/_{h}$ and nozzle position $z = 2\ cm$. As it can be seen from the graph the difference between measured and calculated values of solid mass flow rate is insignificant. It means that the model gives relatively accurate result and the pressure drop coefficient can be considered as accurate enough. Another way of presenting the results of comparing of calculated and measured data is shown on Figure 5-3. From this figure it's clear that the model is accurate enough for calculating solids mass flow rate for vertical air lifters based on pressure drop coefficient K_{st} calculated for instantaneous data from the same experiment.

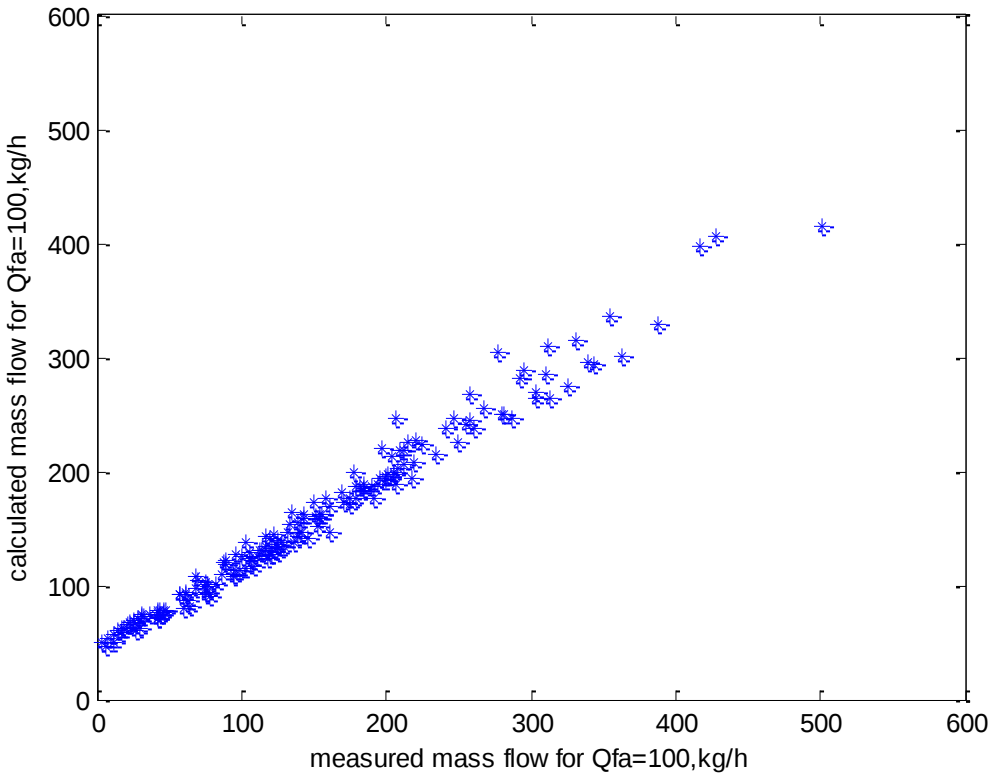

Figure 5-3: Comparing of calculated and measured mass flow rate

Further in this subchapter the dependence of mass flow rate on various parameters is investigated. The model simulations were carried out based on pressure drop coefficient K_{st} calculated from previous experiment (Figure 5-1). To study influence of different operational conditions on solids mass flow rate in vertical air lifters, we decided to do calculations isolating each different operational parameter.

Dependence on $\dot{Q}_{FA}$:

In order to investigate the influence of fluidization air flow rate on mass flow rate of solids in vertical air lifters, the following experimental conditions were considered:

$$\dot{Q}_{FA} = 500\ {}^{m^3}/_{h},\quad \dot{Q}_{TA} = 20\ {}^{m^3}/_{h},\quad z = 2\ cm$$

The Figure 5-4 presents measured mass flow rate vs. calculated mass flow rate for the experiment 500FA 20TA and nozzle position 2 cm based on K_{st} from Figure 5-1.

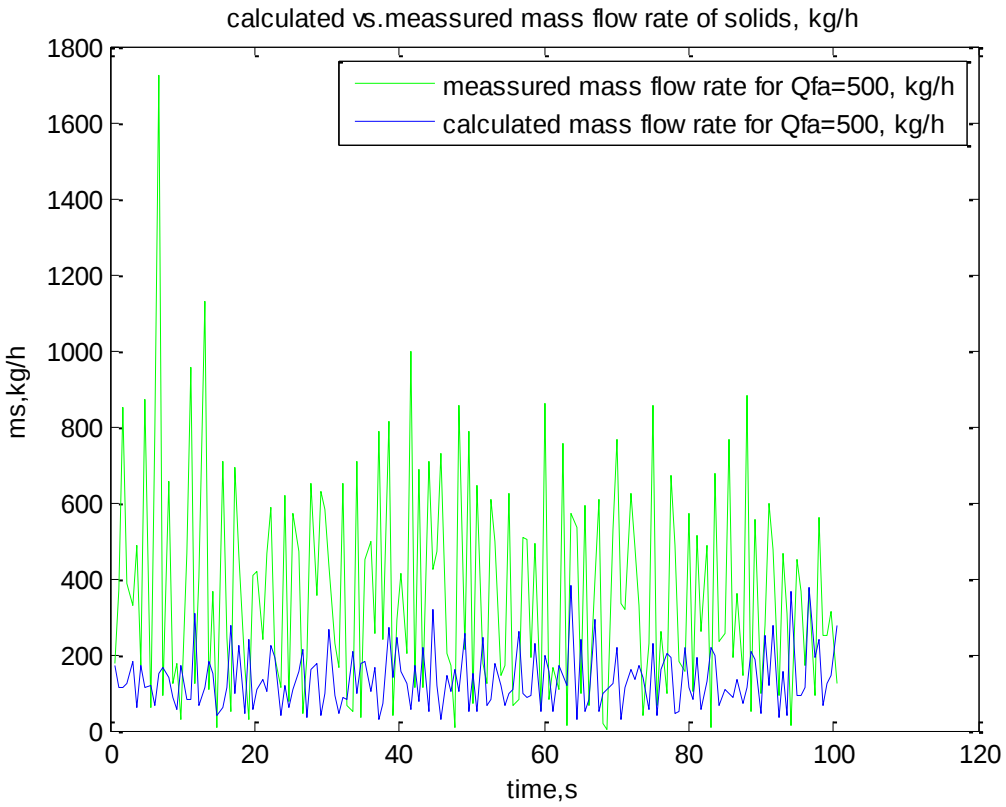

Figure 5-4: Calculated vs. measured mass flow rate for 500FA 20TA 2 cm experiment with zirconium oxide

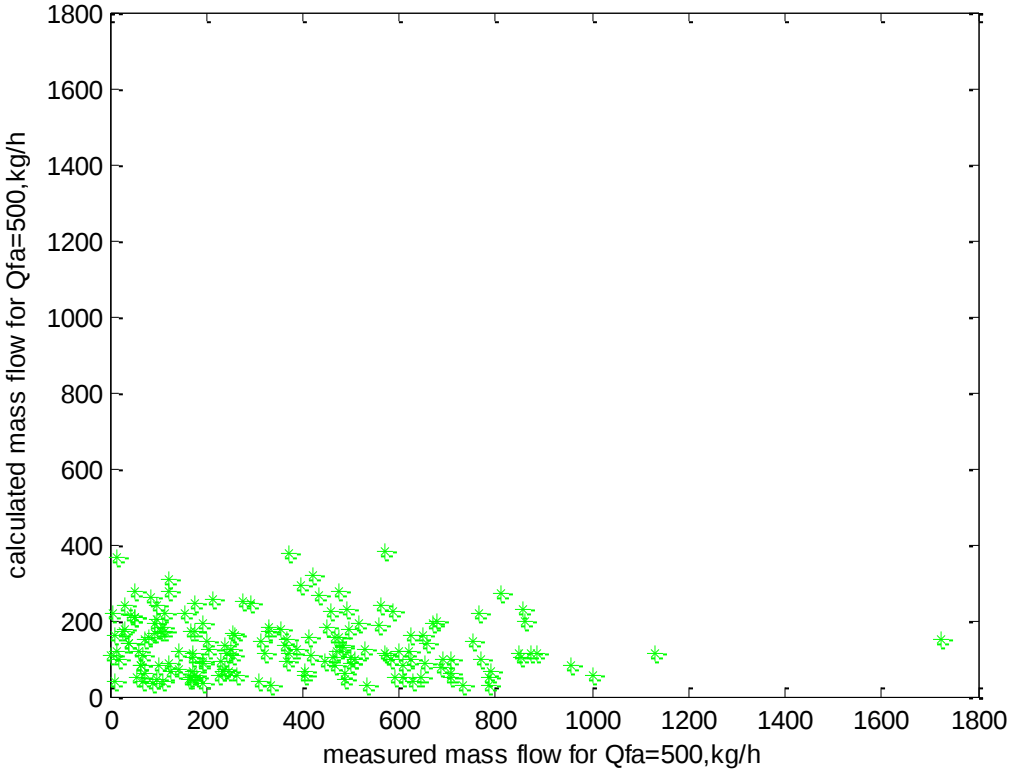

Figure 5-5: Comparing of calculated and measured mass flow rates

As it can be seen, the difference between calculated and measured solids mass flow rate values is significant but the curve that represents calculated mass flow rate has the same shape as the curve which represents measured mass flow rate of solids. As mentioned above it can be concluded that some correction coefficient needs to be added to the model to make the results more suitable for practical implementation.

Dependence on $\dot{Q}_{TA}$:

For the study of influence of the transport air flow rate $\dot{Q}_{TA}$ on mass flow rate of solids in vertical air lifters, the following experimental conditions were analyzed:

$$\dot{Q}_{FA} = 100\ {}^{m^3}/_{h},\quad \dot{Q}_{TA} = 40\ {}^{m^3}/_{h},\quad z = 2\ cm$$

Figure 5-6 and Figure 5-7 show the measured mass flow vs. calculated mass flow rate for the experiment 100FA 40TA and nozzle position 2 cm based on K_{st} from Figure 5-1.

From these figures, it's clearly seen that values of calculated and measured mass flow rate for zirconium oxide are significantly different but the shapes of the curves on Figure 5-6 are similar. It may be explained by model uncertainties which can be avoided by adding the correction coefficient.

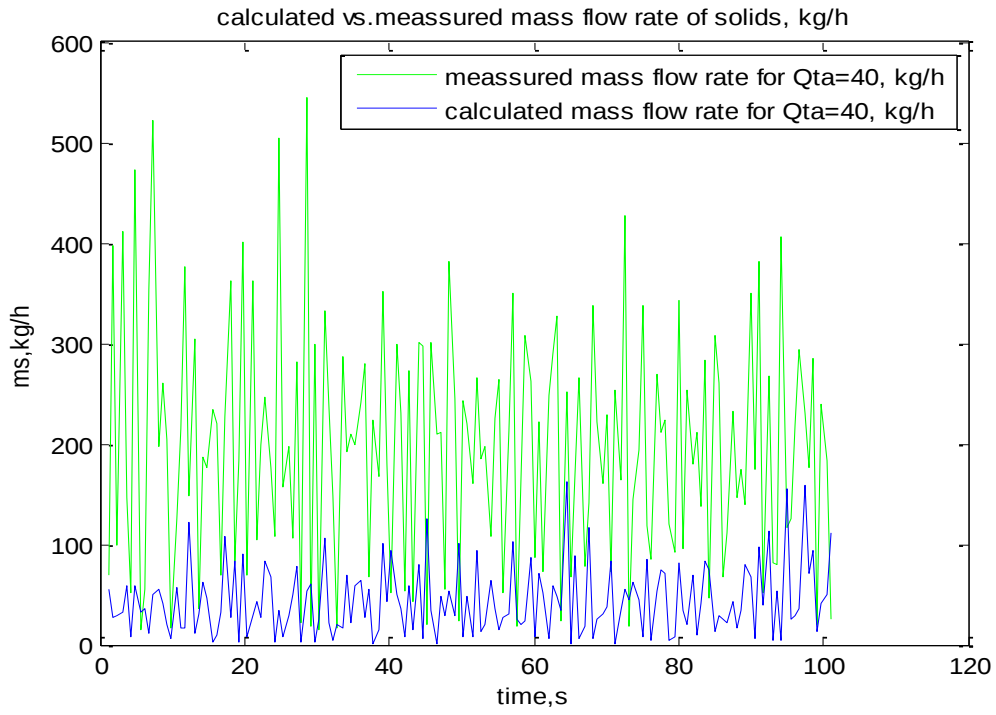

Figure 5-6: Calculated mass flow vs. measured mass flow for 100FA 40TA 2cm experiment with zirconium oxide

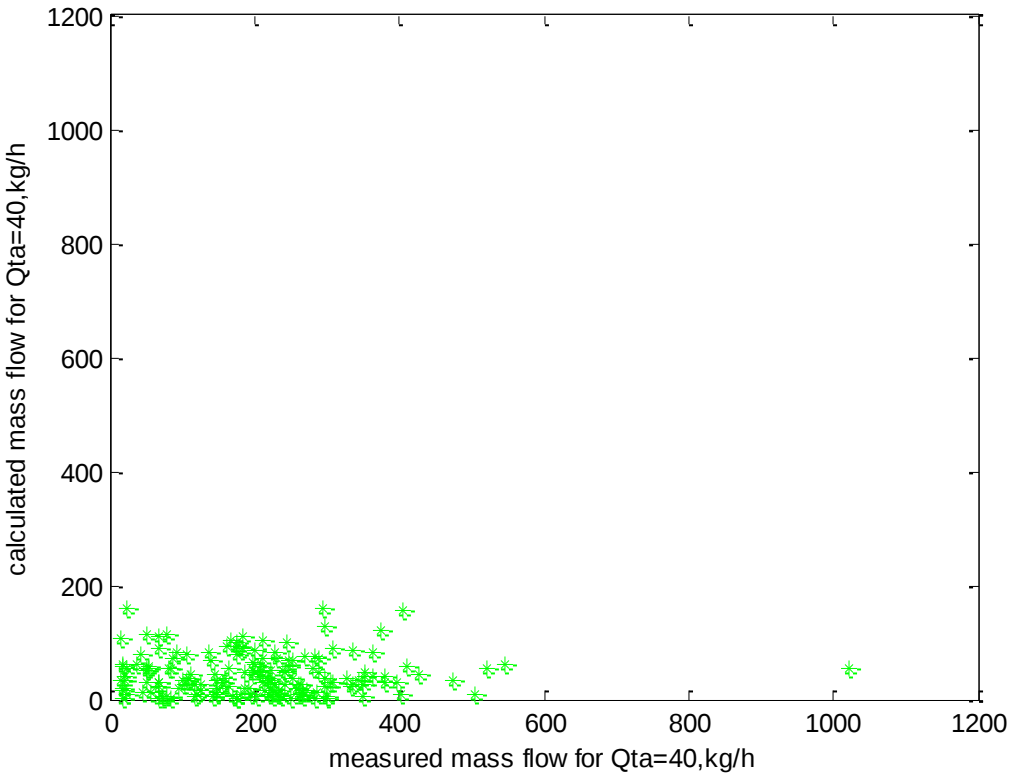

Figure 5-7: Comparing of measured and calculated mass flow rate

Dependence on the nozzle position z:

In order to investigate the influence of the nozzle position z on mass flow rate of solids in vertical air lifters, the following experimental conditions were considered:

$$\dot{Q}_{FA} = 100\ {}^{m^3}/_{h},\quad \dot{Q}_{TA} = 20\ {}^{m^3}/_{h},\quad z = 3\ cm$$

Figure 5-8 and Figure 5-9 represent the comparing of measured mass flow rate and calculated mass flow rate for the experiment 100FA 20TA and nozzle position 3 cm based on K_{st} from Figure 5-1. The difference between calculated and measured mass flow rate of solids can be explained by uncertainties in the model and experimental errors that might occur. It means that model needs to be validated in order to get more accurate result.

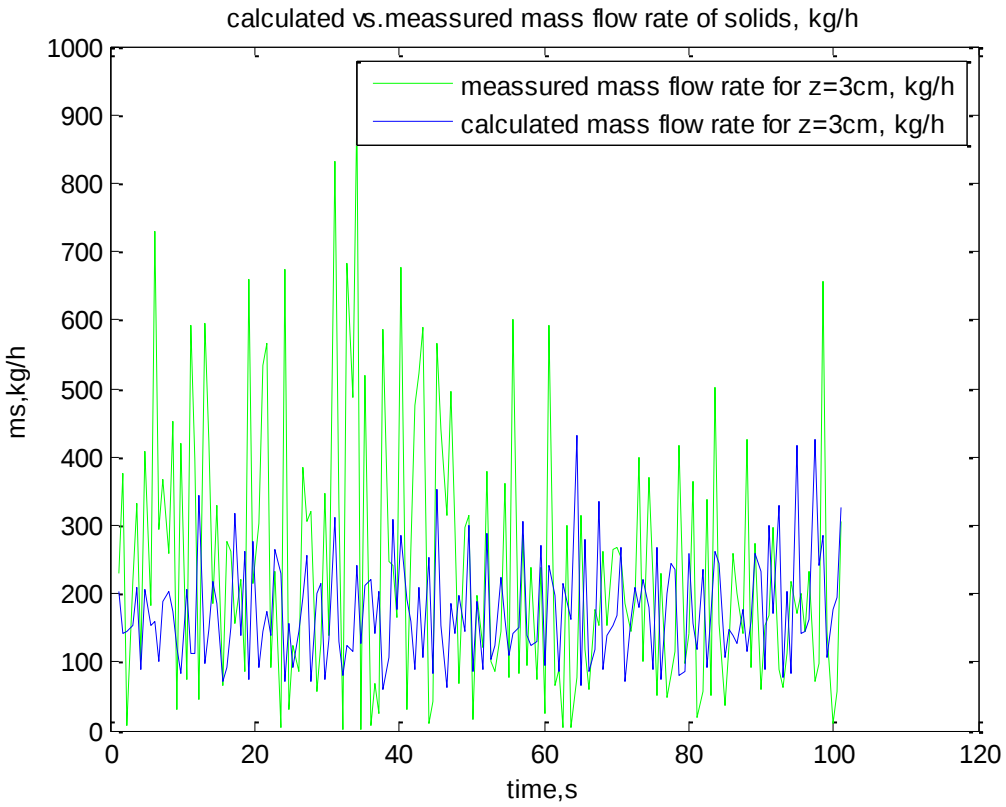

Figure 5-8: Calculated vs. measured mass flow rate for 100FA 20TA 3cm experiment with zirconium oxide

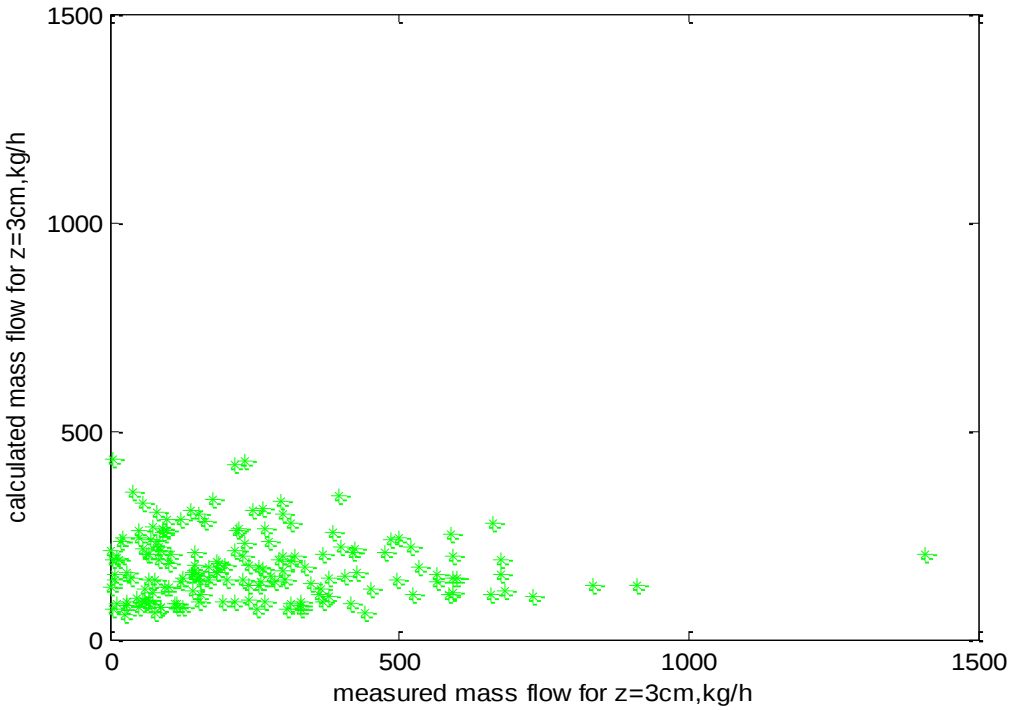

Figure 5-9: Comparing of calculated and measured mass flow rate for 100FA 20TA 3cm experiment with zirconium oxide

Comparison of calculated mass flow rates with respect to different parameters (z, $\dot{Q}_{FA}$, $\dot{Q}_{TA}$) is presented further.

Figure 5-10 shows the calculated mass flow rate for $\dot{Q}_{FA} = 100\ {}^{m^3}/_{h}$, $\dot{Q}_{TA} = 20\ {}^{m^3}/_{h}$ and nozzle position $z = 2cm$ and $z = 3cm$.

As it can be seen from the graph, influence of nozzle position on the mass flow rate of solids in vertical air lifters is not very significant since the values of mass flow for experiments with nozzle position $z = 2cm$ and nozzle position $z = 3cm$ are slightly the same.

Figure 5-11 represents the calculated mass flow rate of solids for $\dot{Q}_{TA} = 20\ {}^{m^3}/_{h}$, $z = 2cm$ and $\dot{Q}_{FA} = 100\ {}^{m^3}/_{h}$ and $\dot{Q}_{FA} = 500\ {}^{m^3}/_{h}$.

It's clear that the influence of fluidization air flow rate on mass flow rate of solids in vertical air lifters is insignificant.

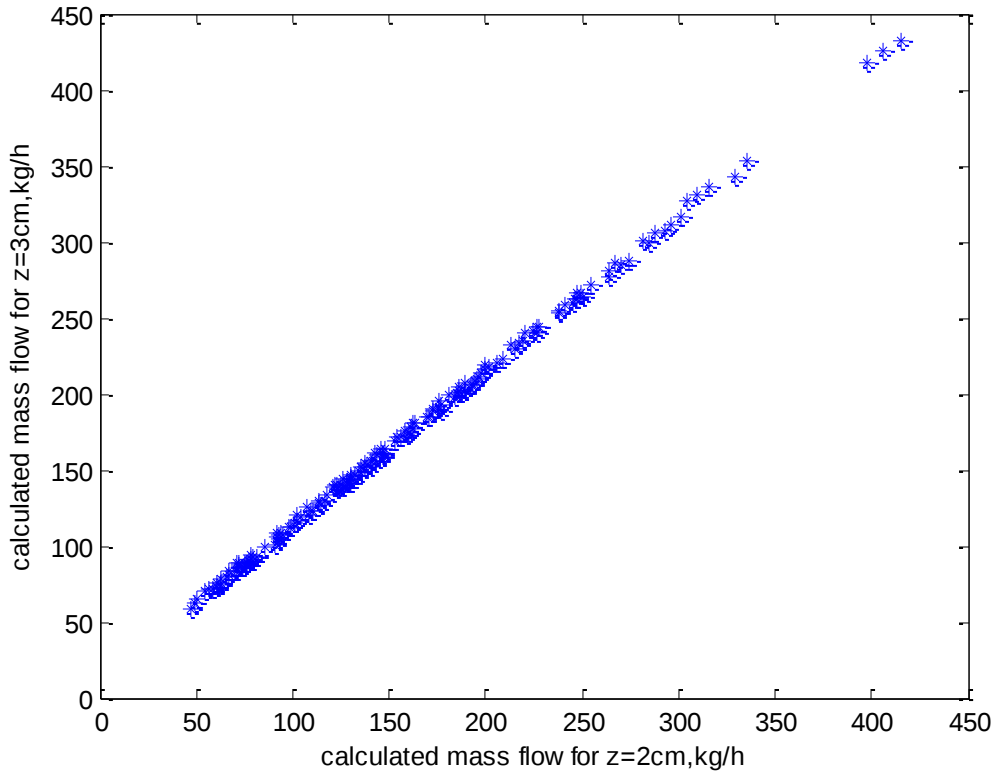

Figure 5-10: Comparing of calculated solid mass flow rate for different nozzle positions z

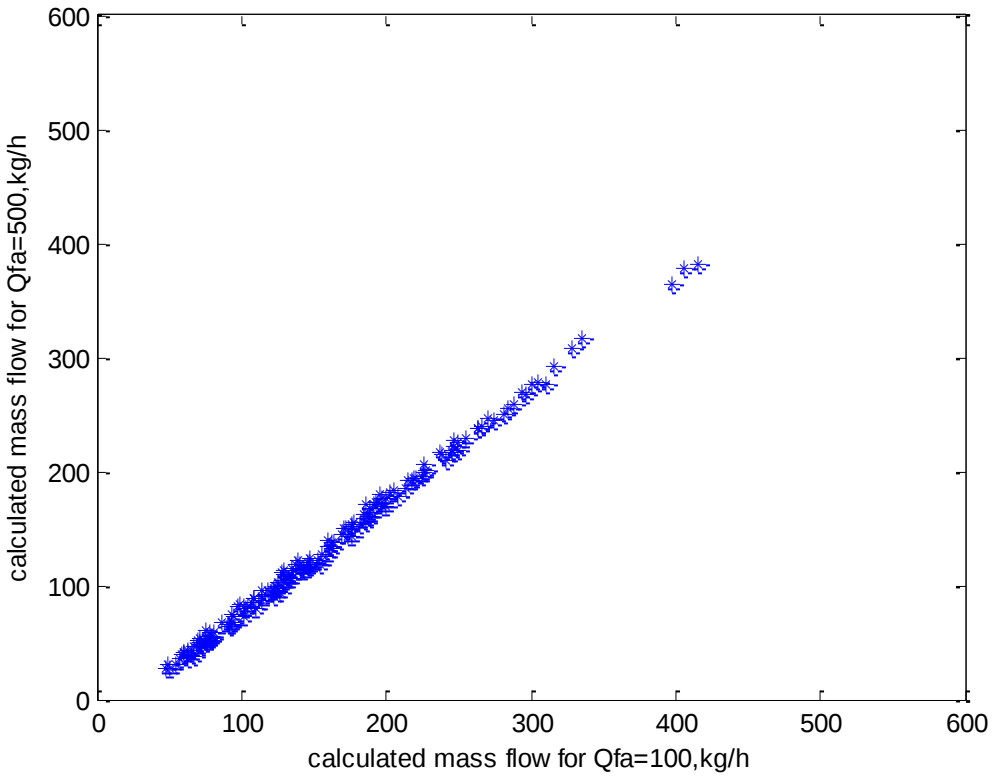

Figure 5-11: Comparing of calculated solid mass flow rates for different Qfa

Figure 5-12 shows the calculated mass flow rate for $\dot{Q}_{FA} = 100\ {}^{m^3}/_{h}$, $z = 2cm$ and $\dot{Q}_{TA} = 20\ {}^{m^3}/_{h}$ and $\dot{Q}_{TA} = 40\ {}^{m^3}/_{h}$. As it can be seen in the graph, the transport air flow rate has the strongest influence on mass flow rate of solids in vertical air lifters.

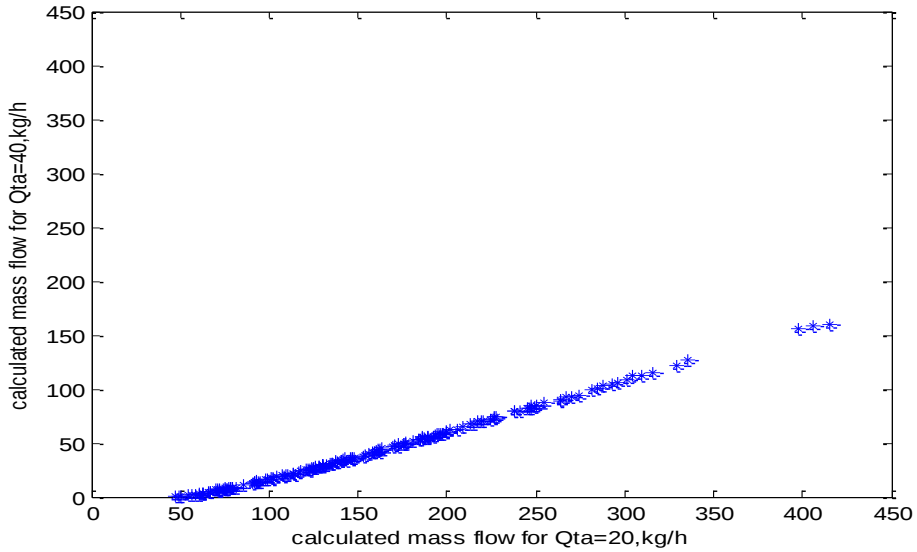

Figure 5-12: Comparing of calculated solid mass flow rates for different Qta

5.2 Average data: zirconium oxide

The following subchapter shows the results of model simulation for experiment with zirconium oxide based on average value of pressure drop coefficient K_{st}.

Figure 5-13 shows the pressure drop coefficient calculated for $\dot{Q}_{FA} = 100\ {}^{m^3}/_{h}$, $\dot{Q}_{TA} = 20\ {}^{m^3}/_{h}$ and nozzle position $z = 2cm$ vs. average pressure drop coefficient.

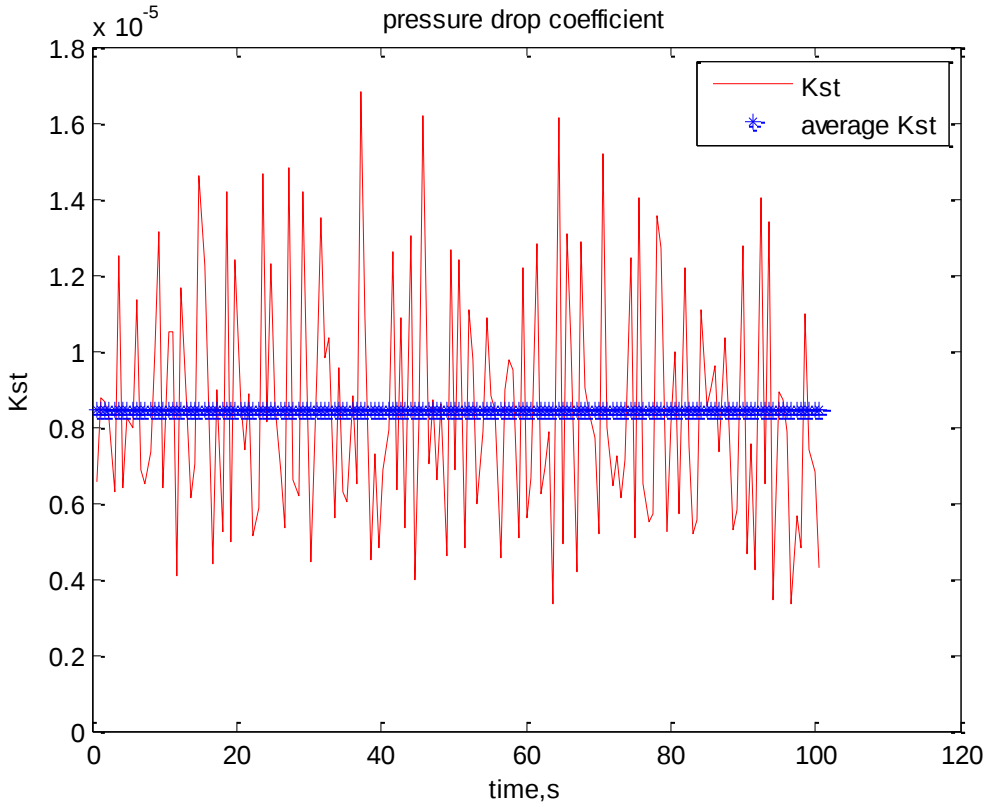

Figure 5-13: Instantaneous vs. average pressure drop coefficient for 100FA 20TA 2cm experiment with zirconium oxide

Average pressure drop coefficient was found for the whole experiment and was used for further calculation of mass flow rate for different conditions.

Figure 5-14 and Figure 5-15 shows the comparison of calculated mass flow rate and measured mass flow rate for experiment with $\dot{Q}_{FA} = 100\ {}^{m^3}/_{h}$, $\dot{Q}_{TA} = 20\ {}^{m^3}/_{h}$ and nozzle position $z = 2cm$ based on average K_{st}. As it is shown in graphs, the difference between measured values of mass flow and values, calculated based on average K_{st}, is significant and the variation of calculated mass flow rate is very small. It's clearly seen that the model gives the result which is slightly stable and it doesn't match with experimental results. It leads to the conclusion that this approach cannot be used with average value of pressure drop coefficient.

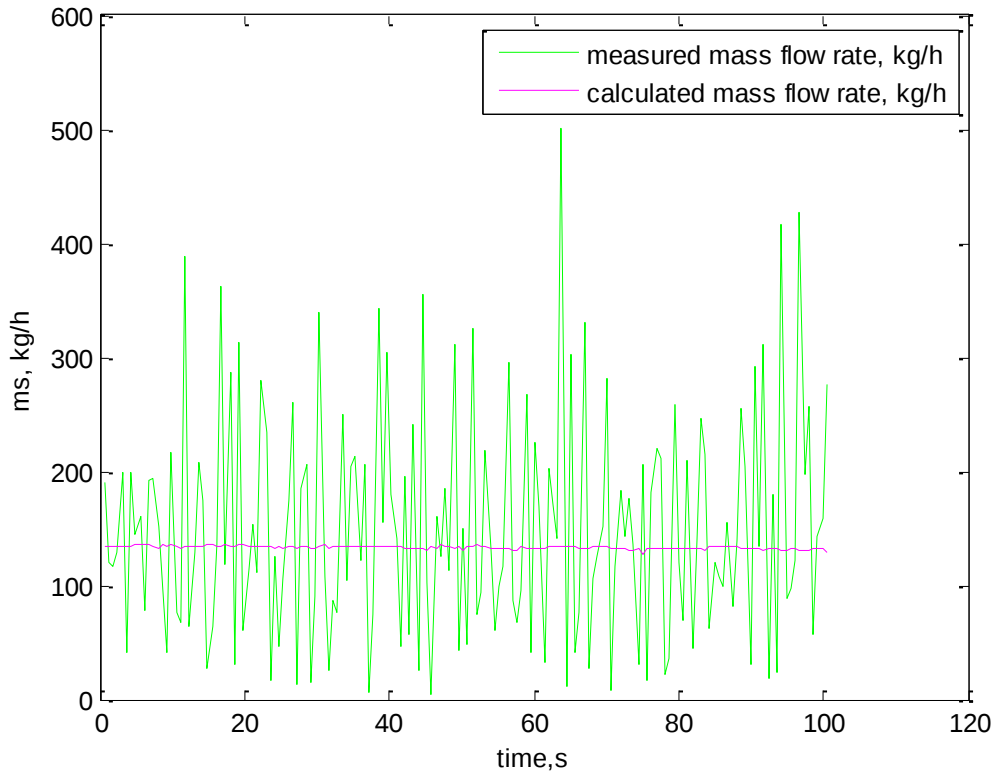

Figure 5-14: Measured vs. calculated mass flow rate for 100FA 20TA z=2cm based on average Kst

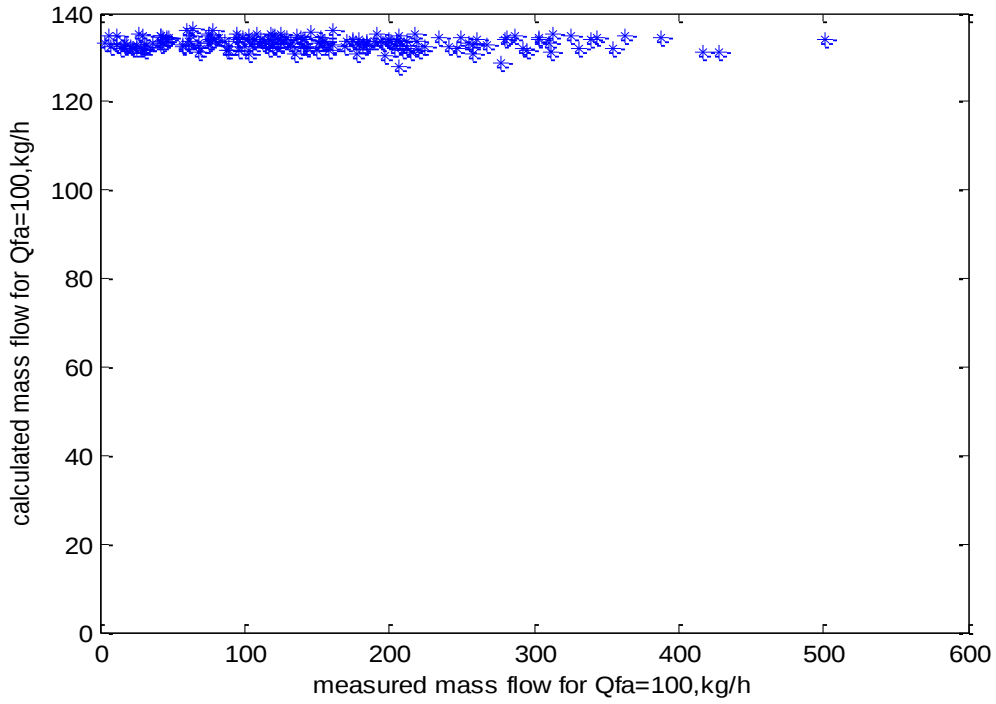

Figure 5-15: Comparing of calculated and measured mass flow rate for 100FA 20TA 2cm experiment with zirconium oxide based on average Kst

Dependence on $\dot{Q}_{FA}$:

In order to investigate the influence of the fluidization air flow rate $\dot{Q}_{FA}$ on mass flow rate of solids in vertical air lifters based on average K_{st}, the experiment was carried out at the following conditions:

$$\dot{Q}_{FA} = 500\ {}^{m^3}/_{h},\ \ \dot{Q}_{TA} = 20\ {}^{m^3}/_{h},\ \ z = 2\ cm$$

Figure 5-16 and Figure 5-17 represent the calculated mass flow rate and measured mass flow rate for experiment with zirconium oxide based on average K_{st}. As the graphs show, the calculated mass flow rate of solids strongly differs from experimental values. It shows the inability to use this model for calculating mass flow rate of solids based on average pressure drop coefficient K_{st}.

As it's shown on Figure 5-18, the calculated mass flow rate of solids can be presented in a form of cluster that proves that model based on average K_{st} isn't accurate and can not be used for prediction of mass flow rate of solids in vertical air lifters.

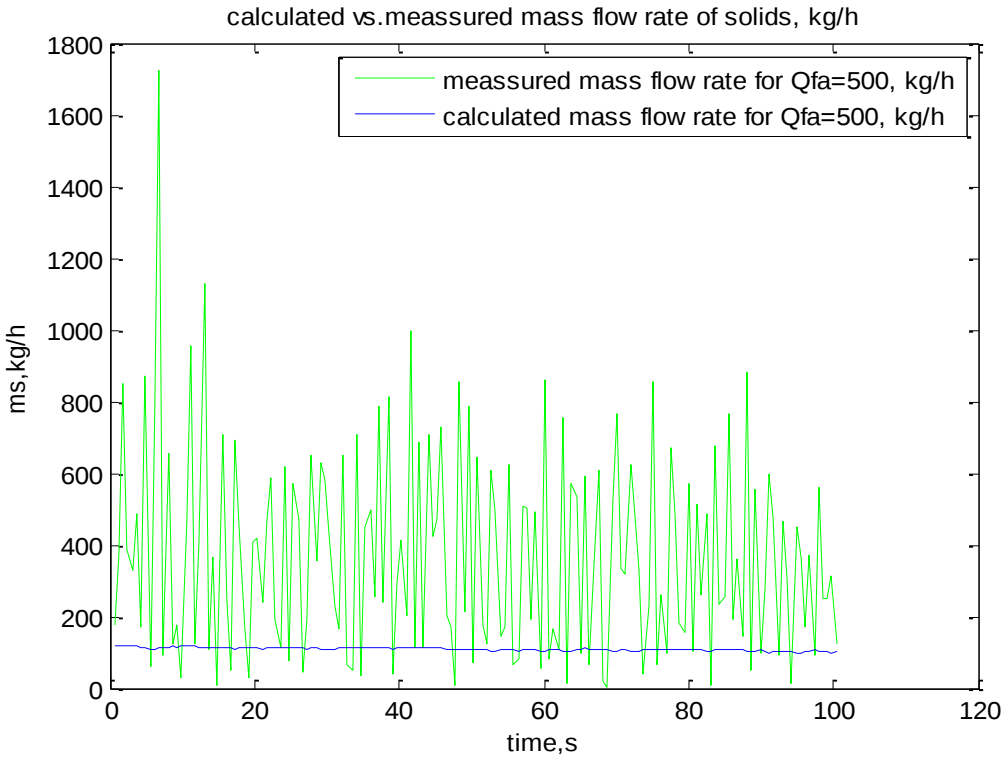

Figure 5-16: Measured vs. calculated mass flow rate for 500FA 20TA z=2cm based on average Kst

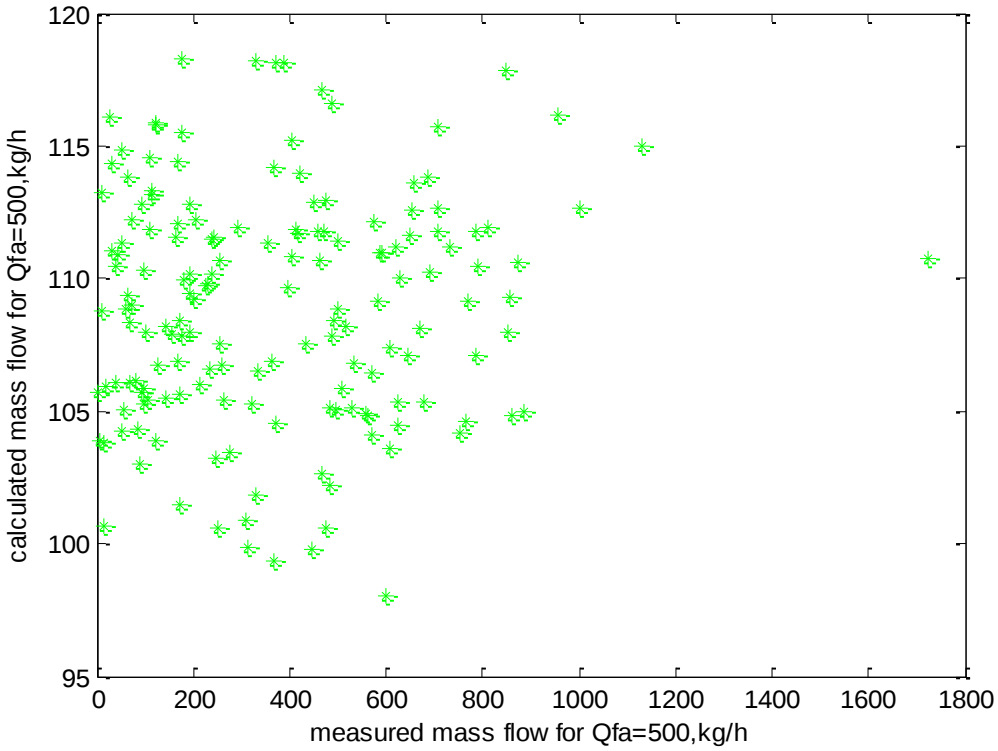

Figure 5-17: Comparing of calculated and measured mass flow rate for 500FA 20TA 2cm experiment with zirconium oxide based on average Kst

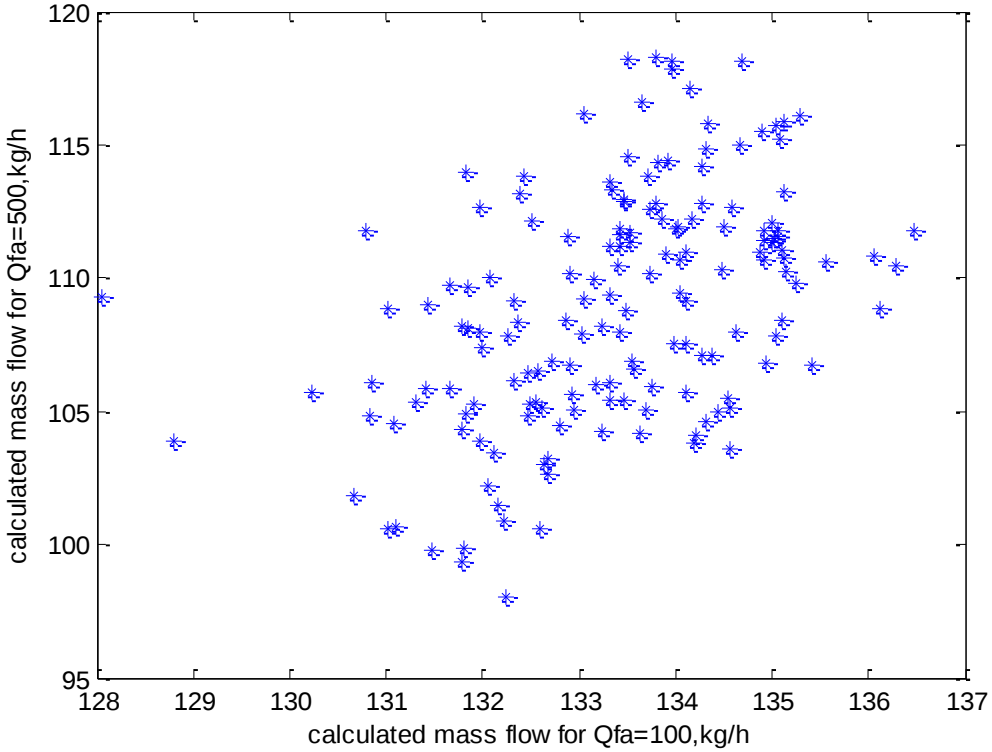

Figure 5-18: Comparing of solid mass flow rate for different Qfa

Dependence on $\dot{Q}_{TA}$:

In order to investigate the influence of the transport air flow rate $\dot{Q}_{TA}$ on mass flow rate of solids in vertical air lifters based on average K_{st}, the experiment was carried out at the following conditions:

$$\dot{Q}_{FA} = 100\ {}^{m^3}/_{h},\ \ \dot{Q}_{TA} = 40\ {}^{m^3}/_{h},\ \ z = 2\ cm$$

It's clear from Figure 5-19 and Figure 5-20, which represents calculated mass flow rate and measured mass flow rate for experiment with zirconium oxide based on average K_{st}, results of model simulation are very different from experimental data. It means that the use of model based on average pressure drop coefficient is inappropriate. Figure 5-21 depicts the point which is stated above since the comparison of calculated results for two different cases is presented as the cluster.

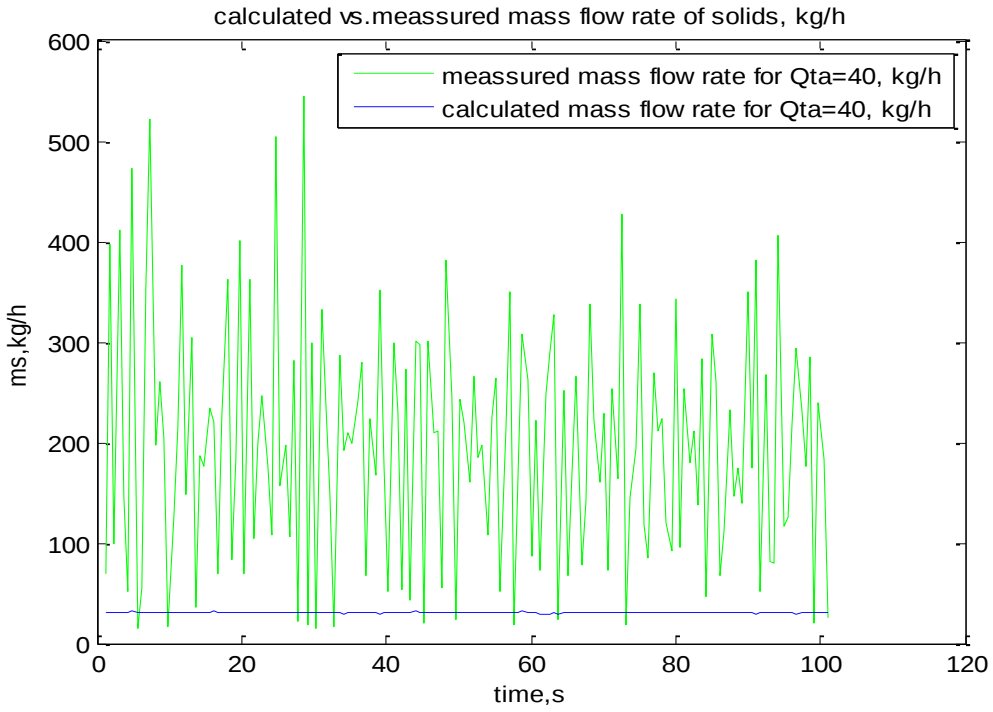

Figure 5-19: Measured vs. calculated mass flow rate for 100FA 40TA z=2cm experiment

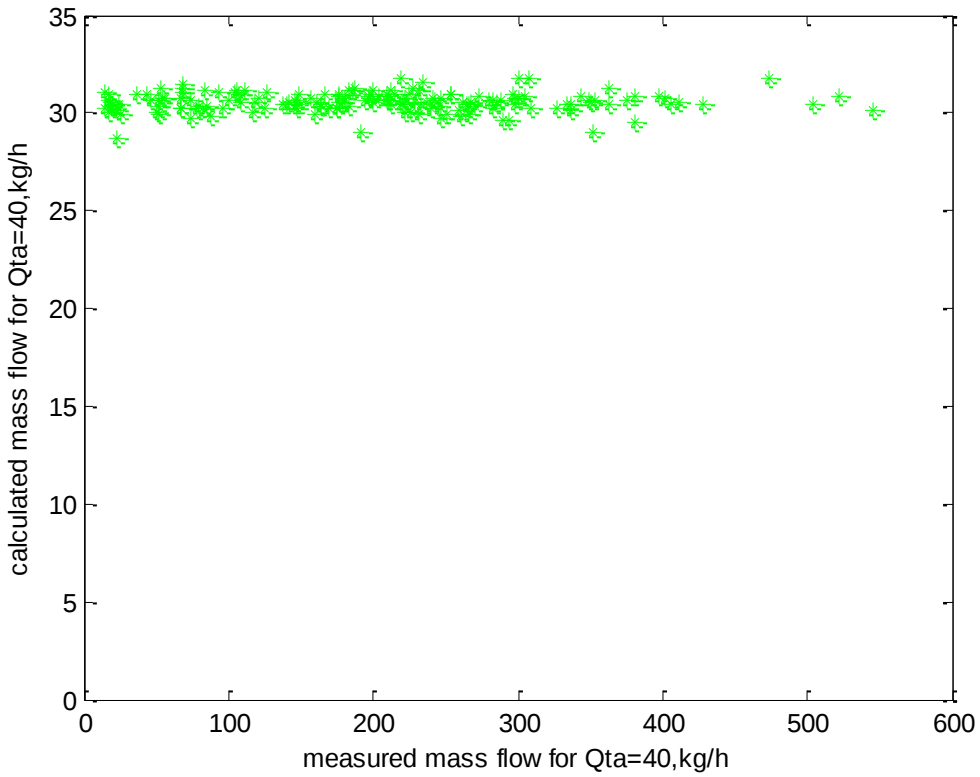

Figure 5-20: Comparing of calculated and measured mass flow rate for 100FA 40TA z=2cm experiment based on average Kst

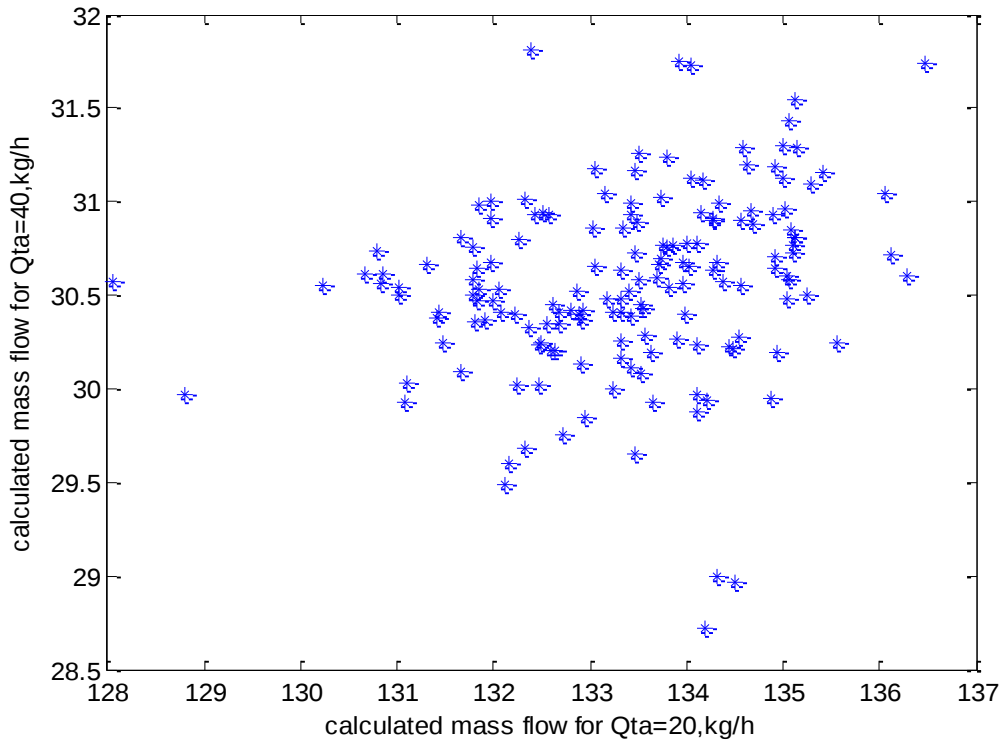

Figure 5-21: Comparing of solid mass flow rate for different Qta

Dependence on the nozzle position z:

In order to investigate the influence of the nozzle position z on mass flow rate of solids in vertical air lifters based on average K_{st}, the experiment was carried out at the following conditions:

$$\dot{Q}_{FA} = 100\ {}^{m^3}/_{h},\quad \dot{Q}_{TA} = 20\ {}^{m^3}/_{h},\quad z = 3\ cm$$

Figure 5-22 and Figure 5-23 show the calculated mass flow rate and measured mass flow rate for experiment with zirconium oxide based on average K_{st}. As it can be seen from the plots, the difference between simulated mass flow rate and experimental data is significant. The comparison of calculated and measured values shows the wide dispersion of data and, as it's presented on Figure 5-24, comparison of simulated mass flow rate for different nozzle position is in clusters form. It can be concluded that the model cannot be used for calculating the solids mass flow rate in vertical air lifters based on average pressure drop coefficient.

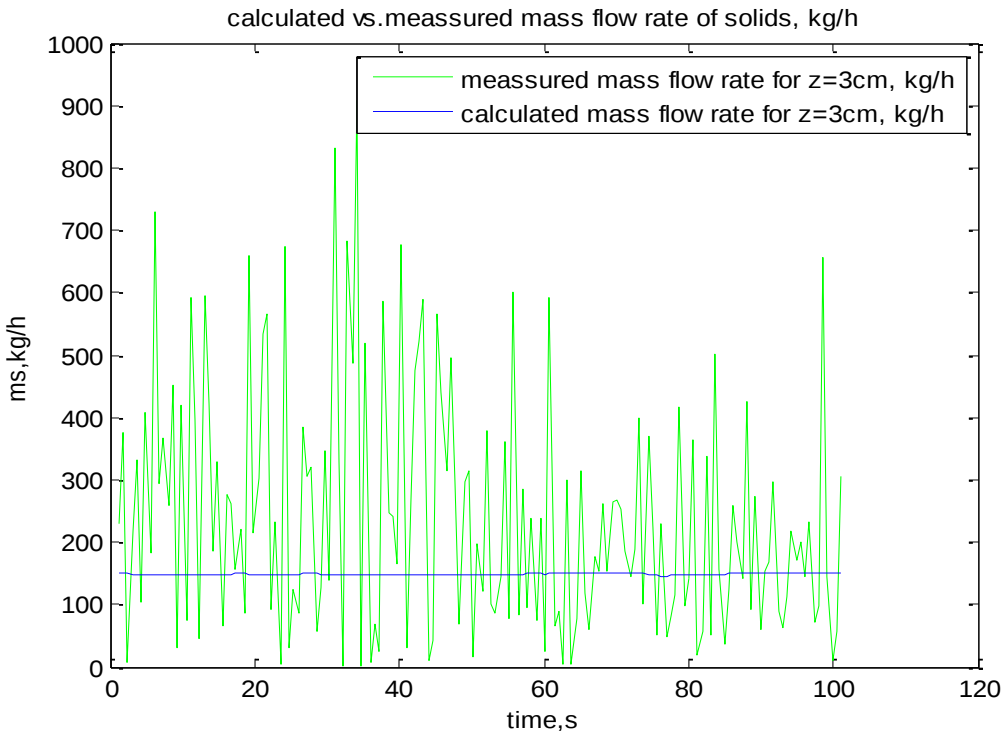

Figure 5-22: Measured vs. calculated mass flow rate for 100FA 20TA z=3cm experiment

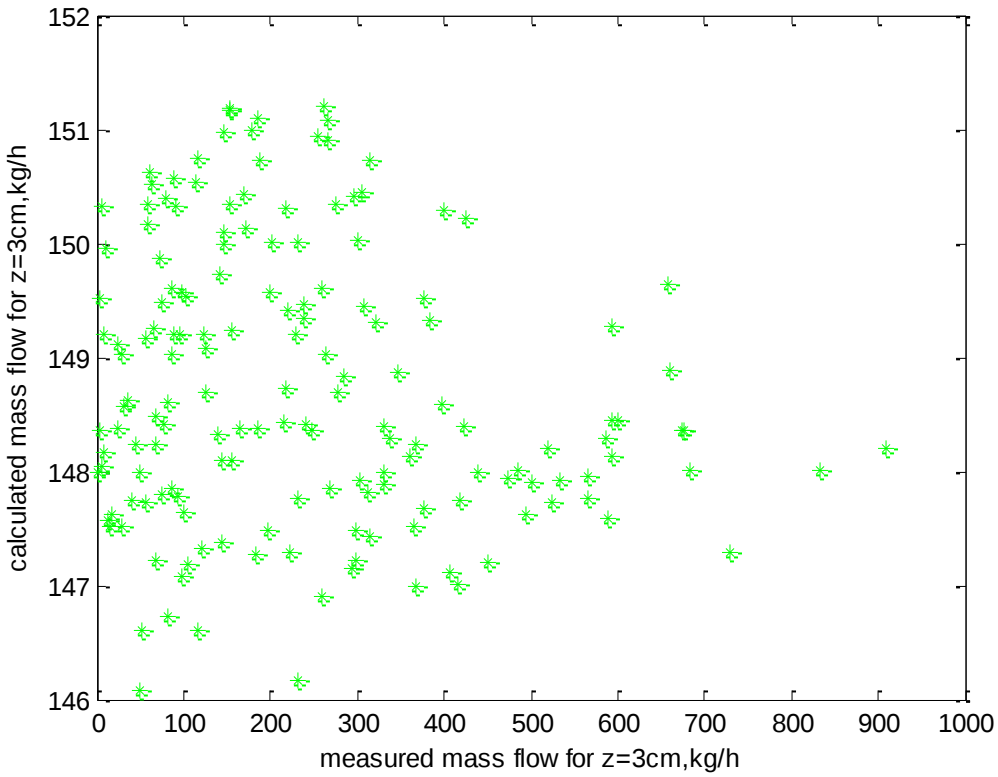

Figure 5-23: Comparing of calculated and measured mass flow rate for 100FA 20TA z=3cm experiment

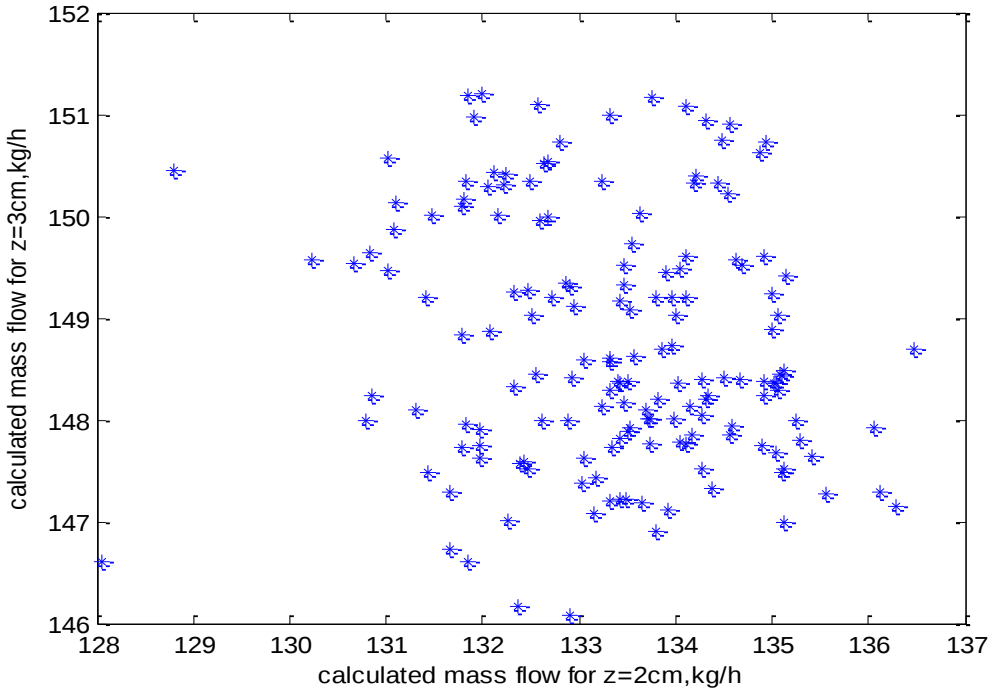

Figure 5-24: Comparing of solid mass flow rate for different nozzle position z

5.3 Average data: glass beads

The following subchapter shows the results of model simulation for experiment with glass beads based on average value of pressure drop coefficient K_{st}.

Pressure drop coefficient calculated for $\dot{Q}_{FA} = 100\ {}^{m^3}/_{h}$, $\dot{Q}_{TA} = 20\ {}^{m^3}/_{h}$, $z = 3\ cm$ vs.

average pressure drop coefficient for the same experiment is presented on Figure 5-25. The average value of pressure drop coefficient K_{st} was used for further calculations of mass flow rate of solids in vertical air lifter at the different conditions.

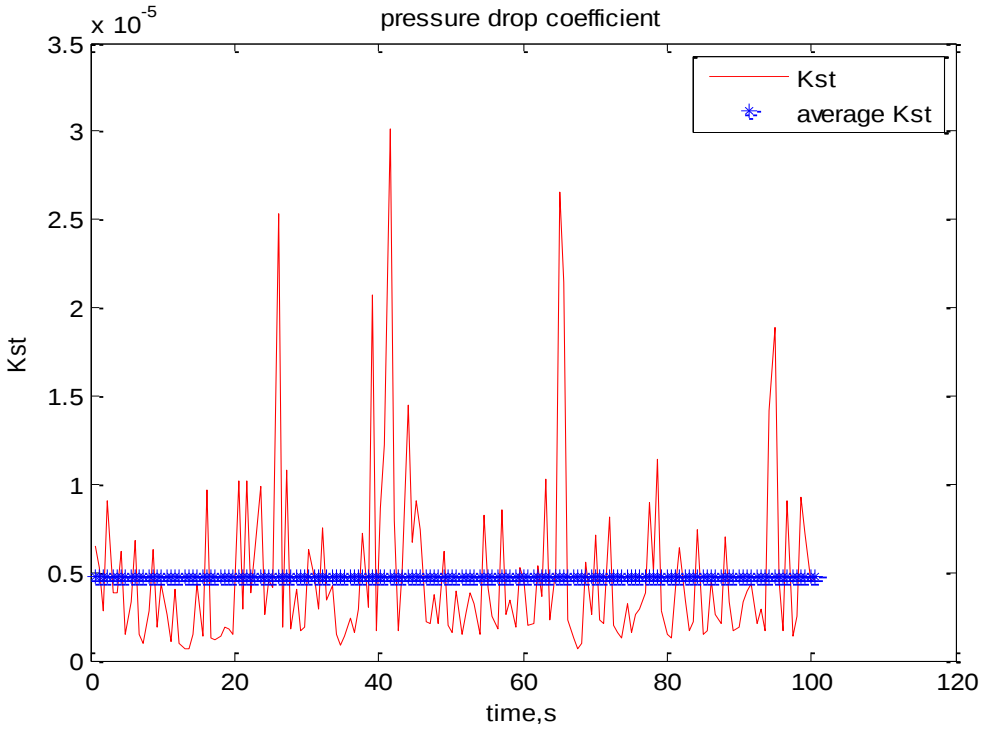

Figure 5-25: Instantaneous and average Kst for glass beads

As it's clearly seen from Figure 5-26 and Figure 5-27 the accuracy of calculated results is low. The dispersion of calculated mass flow with respect to measured data is strong. It leads to conclusion that the model cannot be implemented for prediction of solids mass flow rate in vertical air lifters based on average value of pressure drop coefficient K_{st}. This indicates also that, in case of using average value of K_{st}, model accuracy doesn't depend on material that needs to be transported.

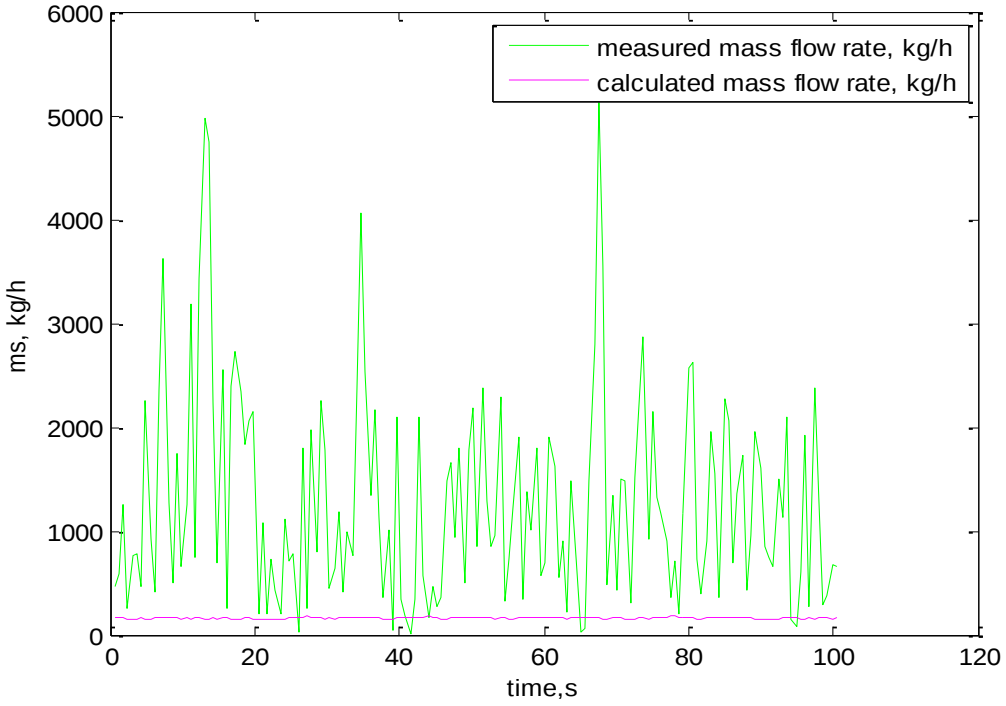

Figure 5-26: Measured vs. calculated mass flow rate for 100FA 20TA 3cm experiment with glass beads

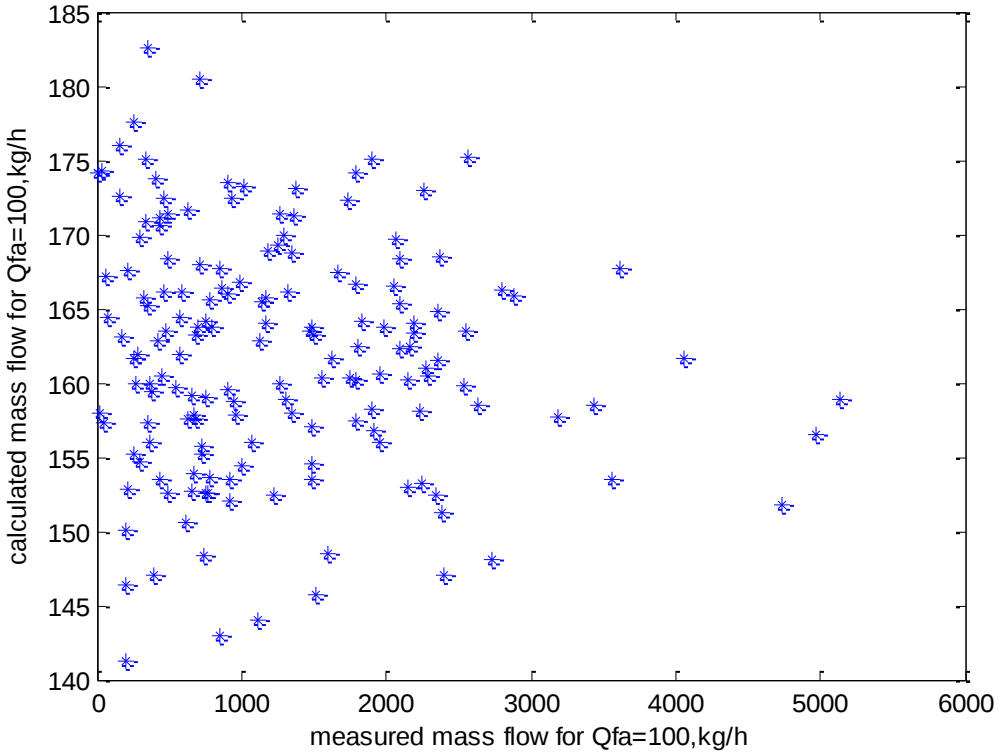

Figure 5-27: Measured vs. calculated mass flow rate for 100FA 20TA 3cm experiment with glass beads

Dependence on $\dot{Q}_{FA}$:

For the investigation of influence of fluidization air flow rate $\dot{Q}_{FA}$ on mass flow rate of glass beads in vertical air lifters based on average K_{st}, the experiment was carried out at the following conditions:

$$\dot{Q}_{FA} = 600\ {}^{m^3}/_{h},\quad \dot{Q}_{TA} = 20\ {}^{m^3}/_{h},\quad z = 3\ cm$$

As it's presented on Figure 5-28 and Figure 5-29 the values of simulated and measured solids mass flow rate are very different. Figure 5-30 shows the wide dispersion of calculated results for $\dot{Q}_{FA} = 600\ {}^{m^3}/_{h}$ with respect to calculated mass flow rate for $\dot{Q}_{FA} = 100\ {}^{m^3}/_{h}$. It indicates that the model is not suitable with averaged value of K_{st}.

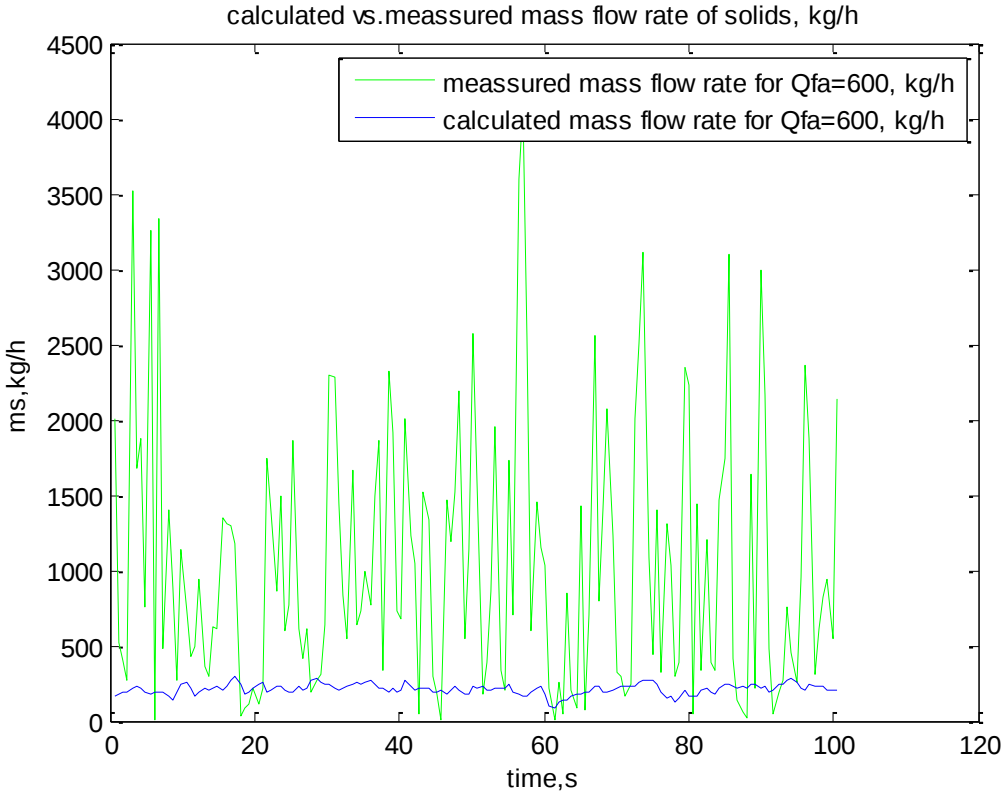

Figure 5-28: Measured vs. calculated mass flow rate for 600FA 20TA 3cm experiment with glass beads

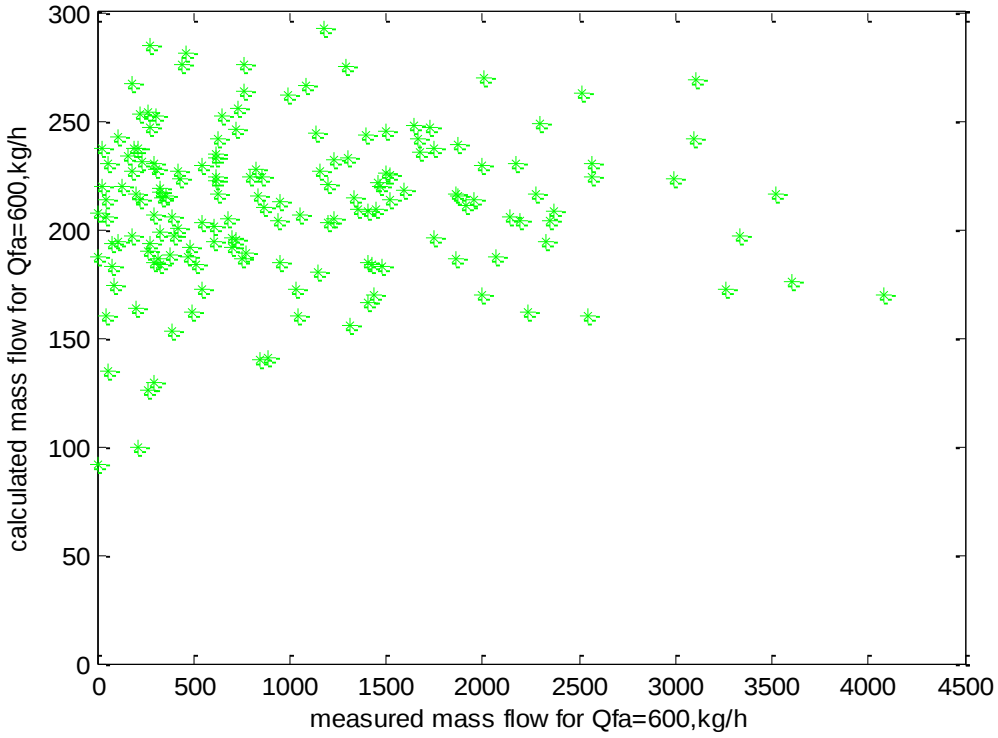

Figure 5-29: Measured vs. calculated mass flow rate for 600FA 20TA 3cm experiment with glass beads

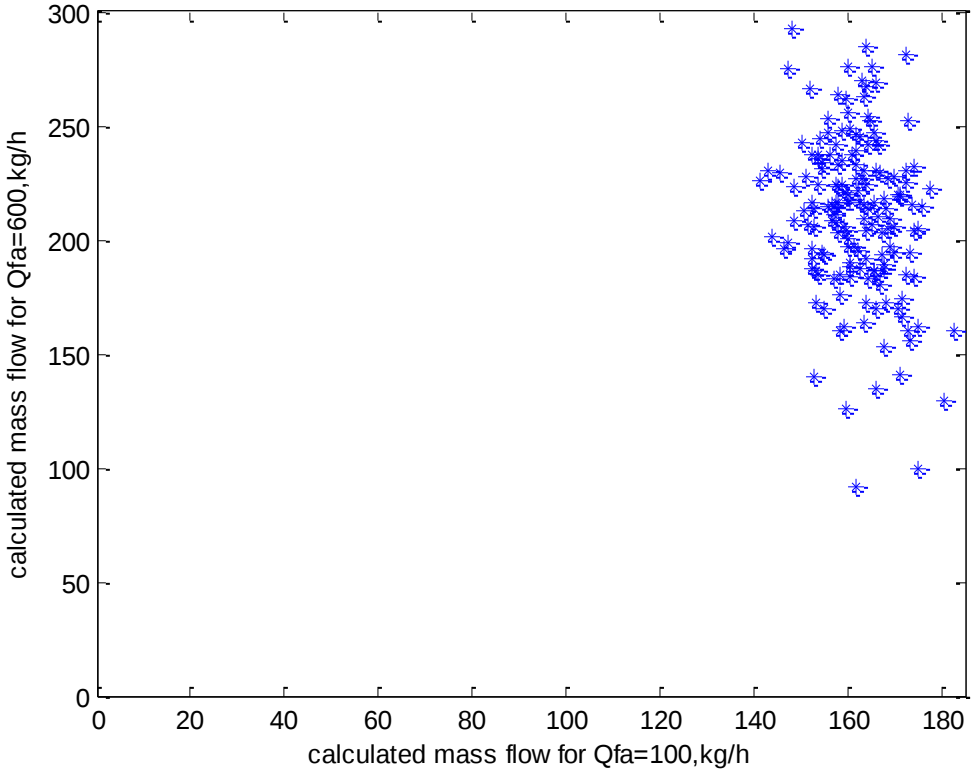

Figure 5-30: Comparing of calculated mass flow rate for different values of Qfa

Dependence on $\dot{Q}_{TA}$:

For the investigation of influence of transport air flow rate $\dot{Q}_{TA}$ on mass flow rate of glass beads in vertical air lifters based on average K_{st}, the experiment was carried out at the following conditions:

$$\dot{Q}_{FA} = 100\ {}^{m^3}/_{h},\ \ \dot{Q}_{TA} = 40\ {}^{m^3}/_{h},\ \ z = 3\ cm$$

It's clear from the Figure 5-31 that simulated values of mass flow rate of solids don't match with experimental data for the same conditions.

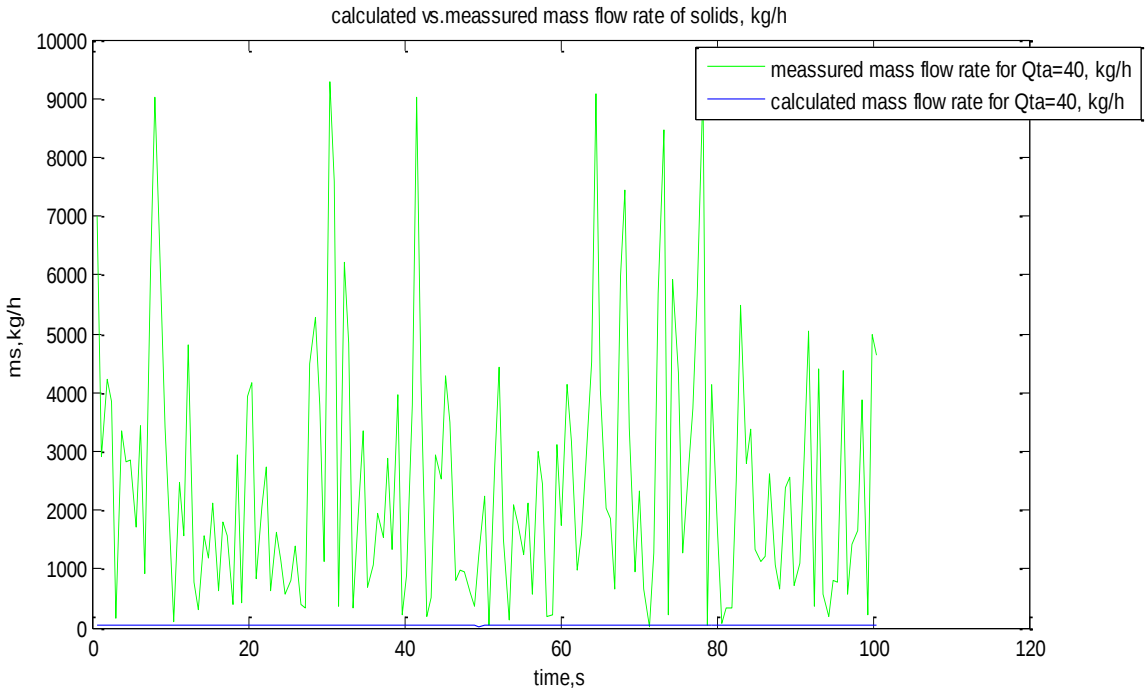

Figure 5-31: Measured vs. calculated mass flow rate for 100FA 40TA 3cm experiment with glass beads

Figure 5-32 shows the distribution of calculated mass flow rate with respect to measured mass flow rate for the same experiment. As it can be seen the values vary significantly. Figure 5-33 presents the comparison of calculated mass flow rate of solids for different values of transport air flow rate $\dot{Q}_{TA}$. Since the simulated mass flow rate of glass beads is widely dispersed in a form of cluster, it leads to the conclusion that the developed model cannot be applied for prediction of mass flow rate of solids in vertical air lifters based on average pressure drop coefficient K_{st}.

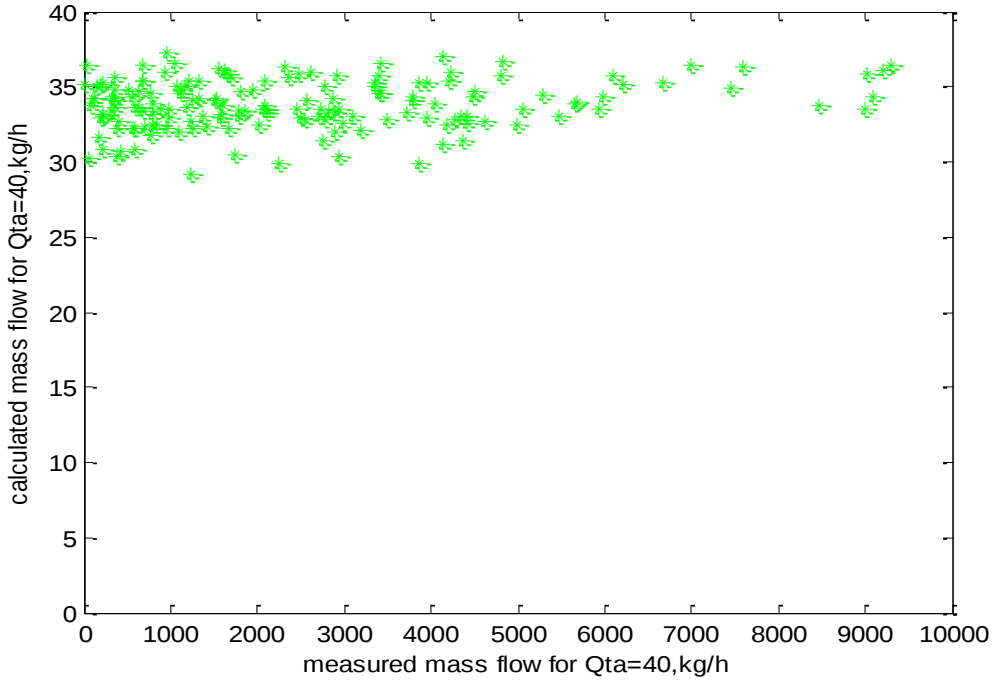

Figure 5-32: Measured vs. calculated mass flow rate for 100FA 40TA 3cm experiment with glass beads

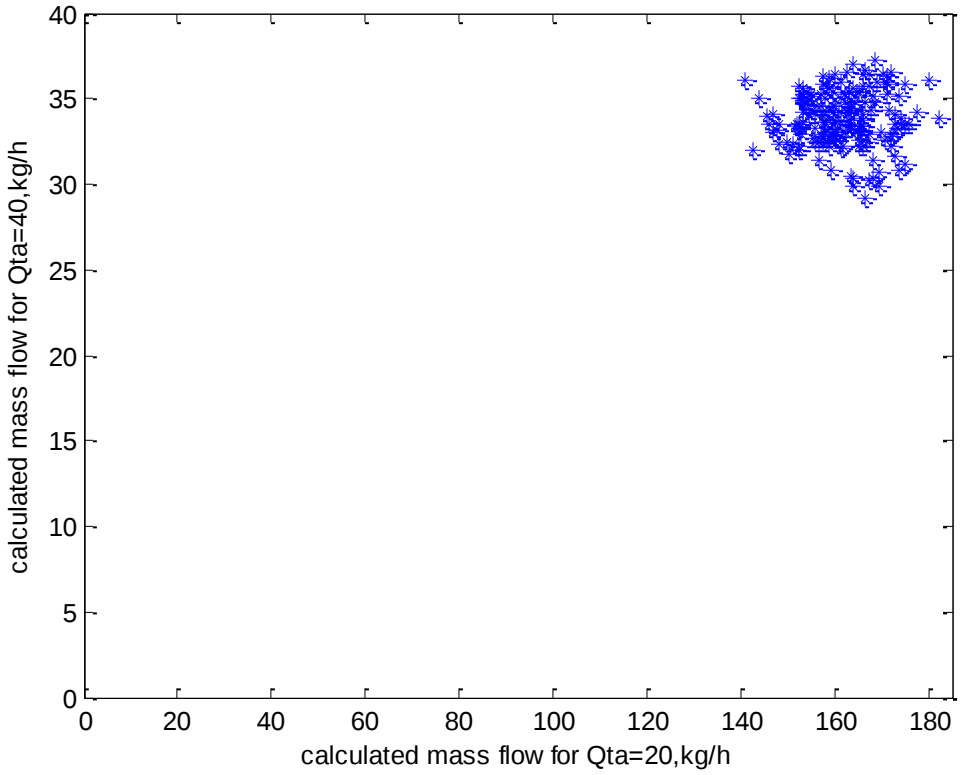

Figure 5-33: Calculated mass flow rate for different values of Qta

5.4 Instantaneous data: glass beads

The following subchapter shows the results of model simulation for experiment with glass beads based on instantaneous data.

Pressure drop coefficient, which is presented on Figure 5-34, calculated for $\dot{Q}_{FA} = 100\ {}^{m^3}/_{h}$, $\dot{Q}_{TA} = 20\ {}^{m^3}/_{h}$ and nozzle position $z = 3cm$ for experiment with glass beads. If to compare the values of pressure drop coefficient for zirconium oxide (Figure 5-1) with the values of pressure drop coefficient for glass beads (Figure 5-34) at the all other similar conditions, it can be concluded that the range of K_{st} for zirconium oxide is higher than the range of K_{st} in experiment with glass beads.

The calculated and measured mass flow rates of solids for the experiment with glass beads are shown on Figure 5-35. As it can be seen, the curves which represent the measured and calculated mass flow are very similar but the values of mass flow rate are slightly different. It can be caused by the experimental errors and model uncertainties and it can be avoided by validation and calibration of model.

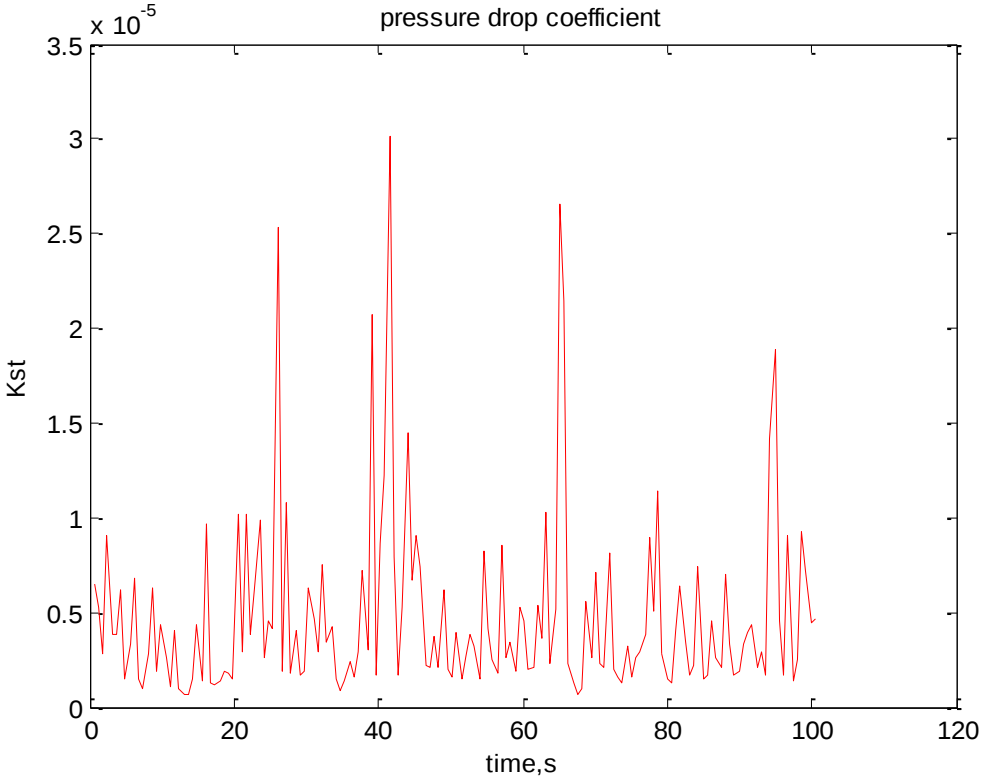

Figure 5-34: Pressure drop coefficient

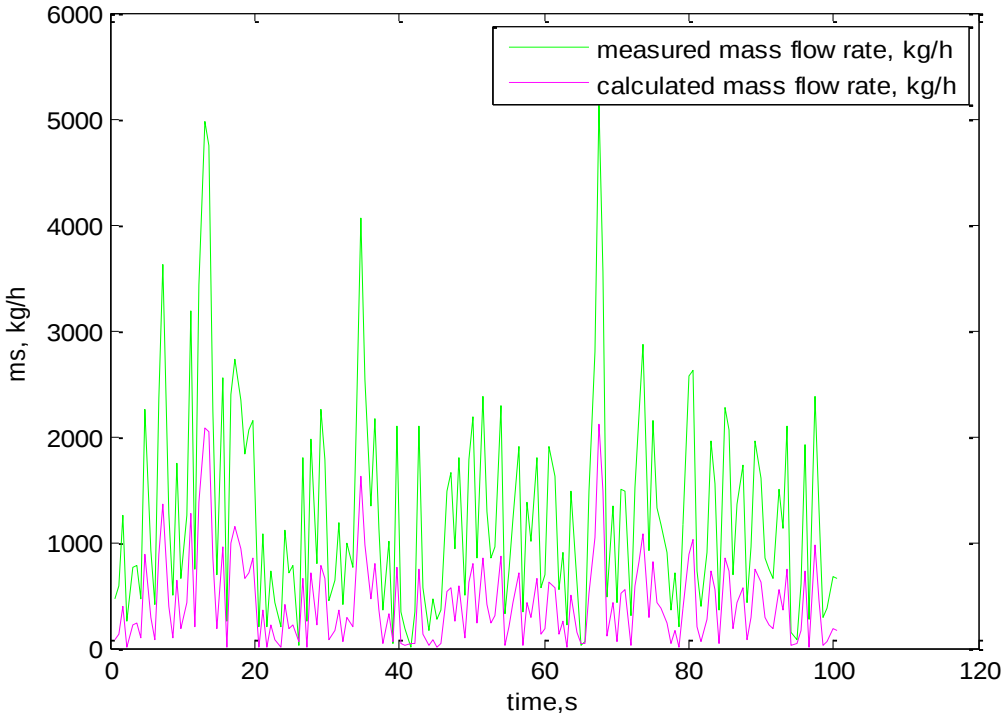

Figure 5-35: Measured vs. calculated mass flow rate for 100FA 20TA 3cm experiment with glass beads

Another way of presenting the comparison of calculated and measured mass flow rates for the experiment with glass beads is shown on Figure 5-36.

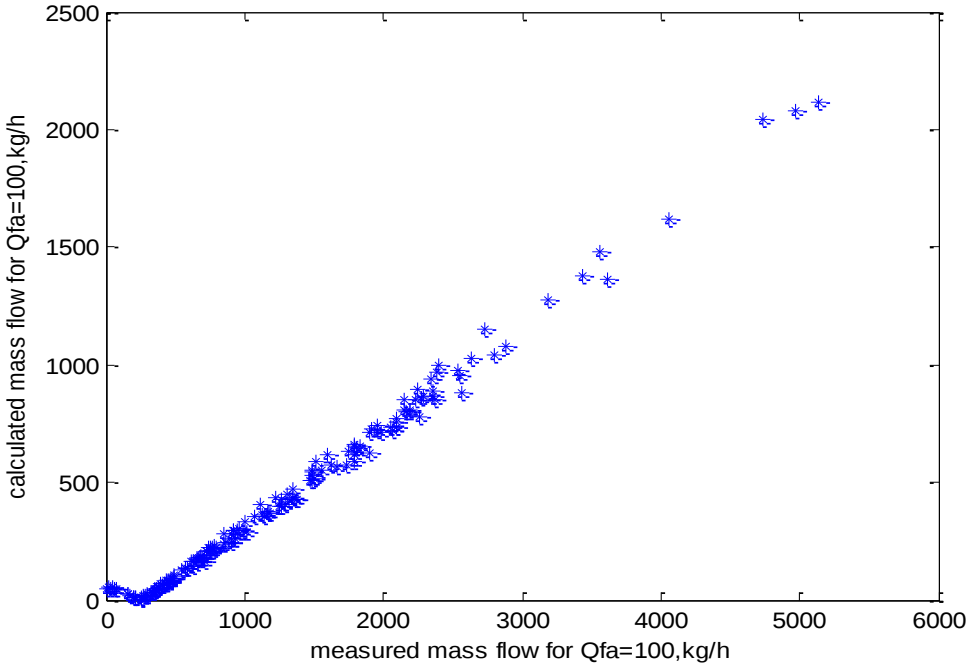

Figure 5-36: Measured vs. calculated mass flow rate for 100FA 20TA 3cm experiment with glass beads

Dependence on $\dot{Q}_{FA}$:

For the study of influence of the fluidization air flow rate $\dot{Q}_{FA}$ on mass flow rate of solids in vertical air lifters, the experiment was carried out at the following conditions:

$$\dot{Q}_{FA} = 600\ {}^{m^3}/_{h},\ \ \dot{Q}_{TA} = 20\ {}^{m^3}/_{h},\ \ z = 3\ cm$$

As it can be seen in Figure 5-37 and Figure 5-38, the difference between calculated and measured mass flow rate of solids in experiment with glass beads is significant but the shape of the curves is relatively similar. It means that the model can be used for calculating the mass flow rate of solids in vertical air lifters but it requires adding the correction coefficient.

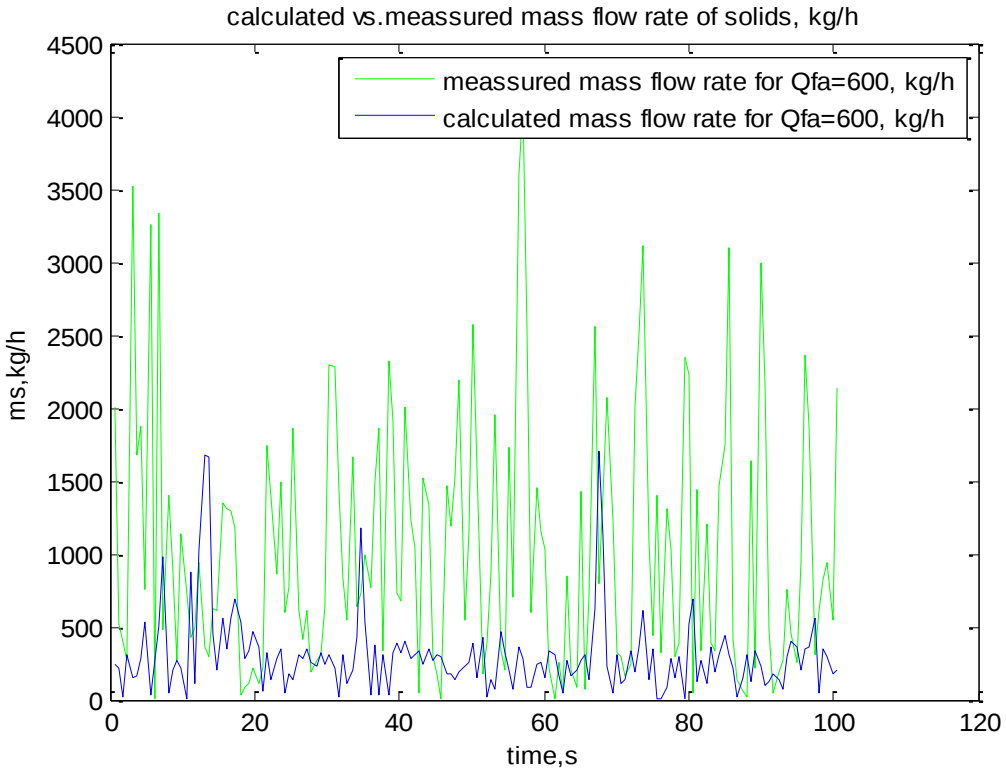

Figure 5-37: Measured vs. calculated mass flow rate for 600FA 20TA 3cm experiment with glass beads

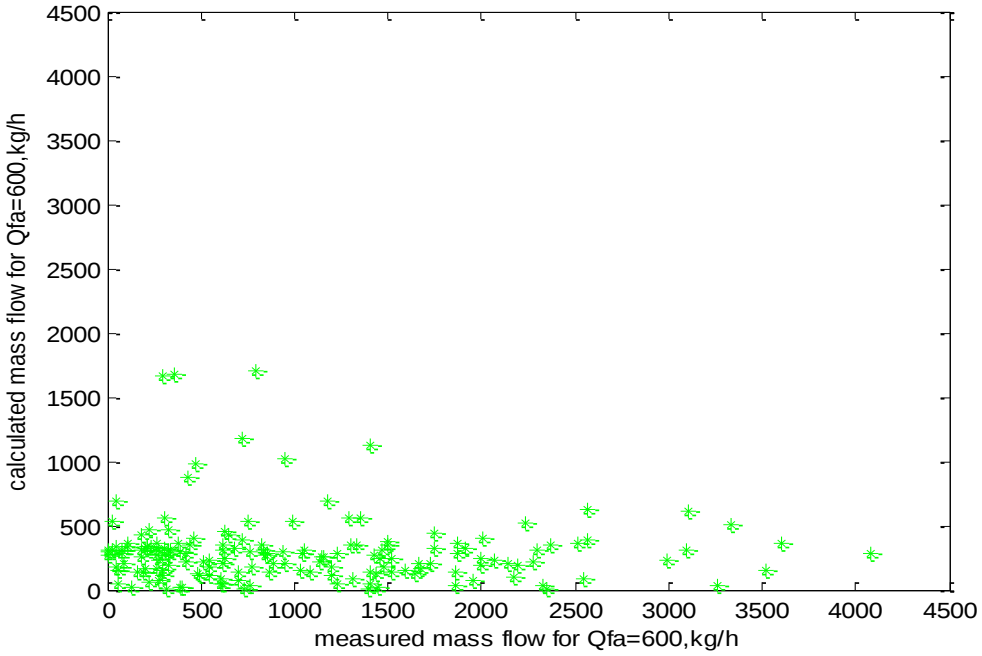

Figure 5-38: Measured vs. calculated mass flow rate for 600FA 20TA 3cm experiment with glass beads

Figure 5-39 shows the comparison of calculated mass flow rates of solids for experiment with glass beads and different values of $\dot{Q}_{FA}$. It's clear from the graph that the values of mass flow calculated for $\dot{Q}_{FA} = 600\,{}^{m^3}/_{h}$ are close to values of mass flow rate calculated for $\dot{Q}_{FA} = 100\,{}^{m^3}/_{h}$. This indicates that the fluidization air flow rate slightly influence on mass flow rate of solids in vertical air lifters.

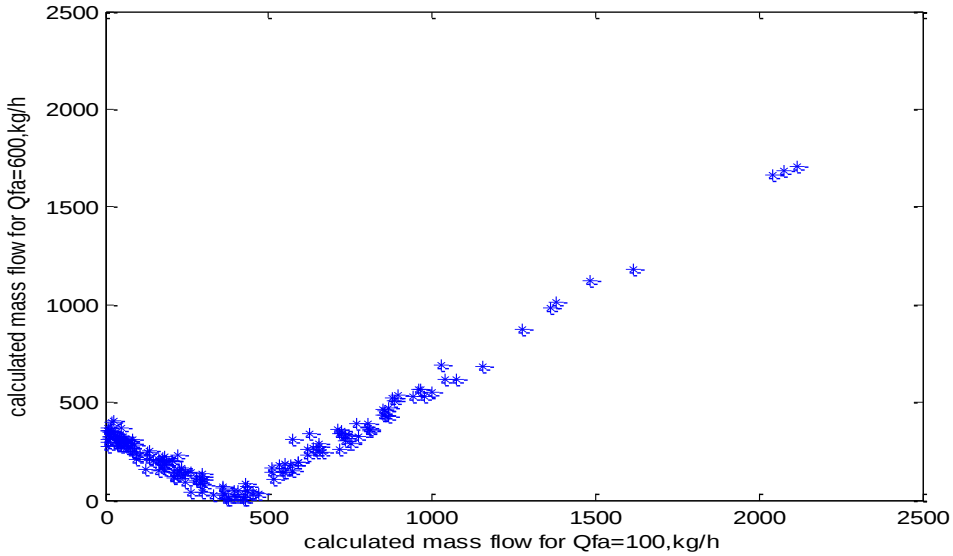

Figure 5-39: Calculated mass flow rate for different values of Qfa

Dependence on $\dot{Q}_{TA}$:

In order to study of influence of the fluidization air flow rate $\dot{Q}_{FA}$ on mass flow rate of glass beads in vertical air lifters, the experiment was carried out at the following conditions:

$$\dot{Q}_{FA} = 100\ {}^{m^3}/_{h},\ \ \dot{Q}_{TA} = 40\ {}^{m^3}/_{h},\ \ z = 3\ cm$$

Figure 5-40 and Figure 5-41 show the calculated and measured mass flow rate of glass beads. As it can be seen from the graphs, the difference between values of mass flow rate is significant. It may occur due to the model uncertainties and experimental errors and can be avoided by adding the correction coefficient into the model. Model needs to be validated and calibrated in order to get more accurate result.

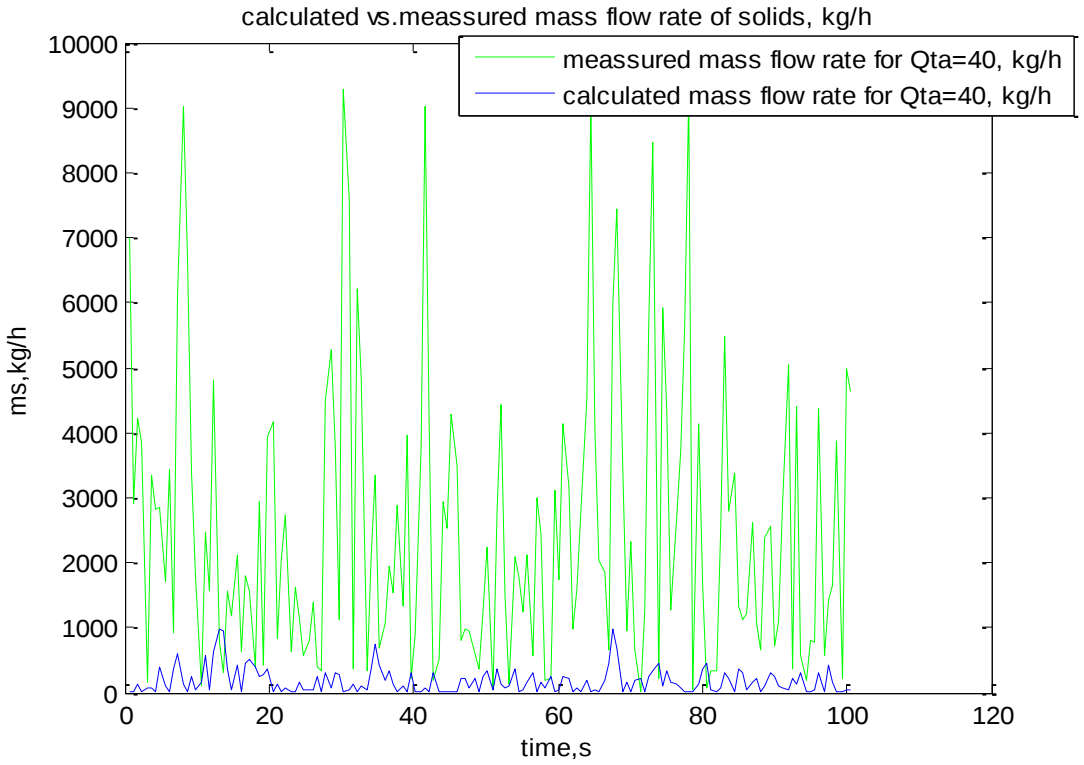

Figure 5-40: Measured vs. calculated mass flow rate for 100FA 40TA 3cm experiment with glass beads

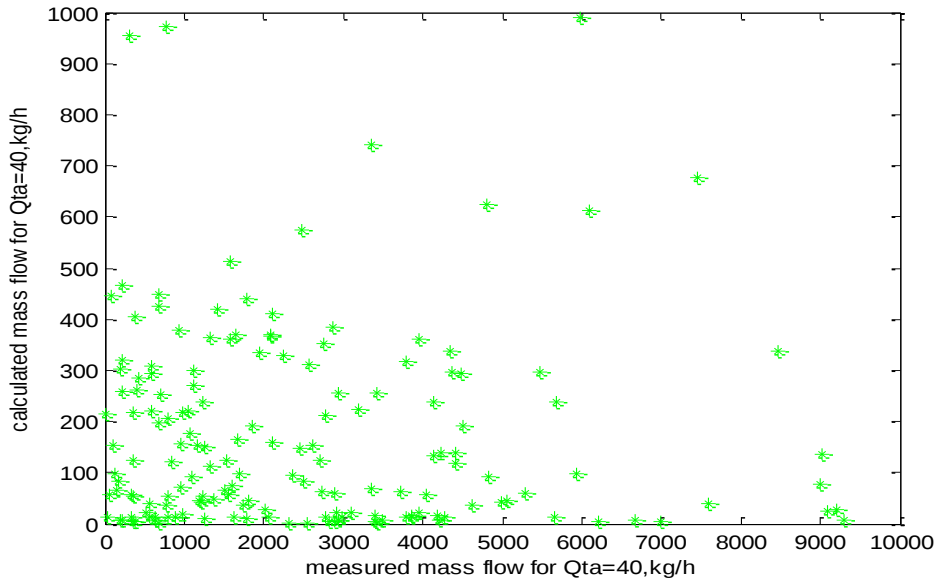

Figure 5-41: Measured vs. calculated mass flow rate for 100FA 40TA 3cm experiment with glass beads

Comparison of calculated mass flow rates for different values of $\dot{Q}_{TA}$ presented on Figure 5-42. It's clear from the graph that transport air flow rate slightly influence on mass flow rate of solids in vertical air lifters.

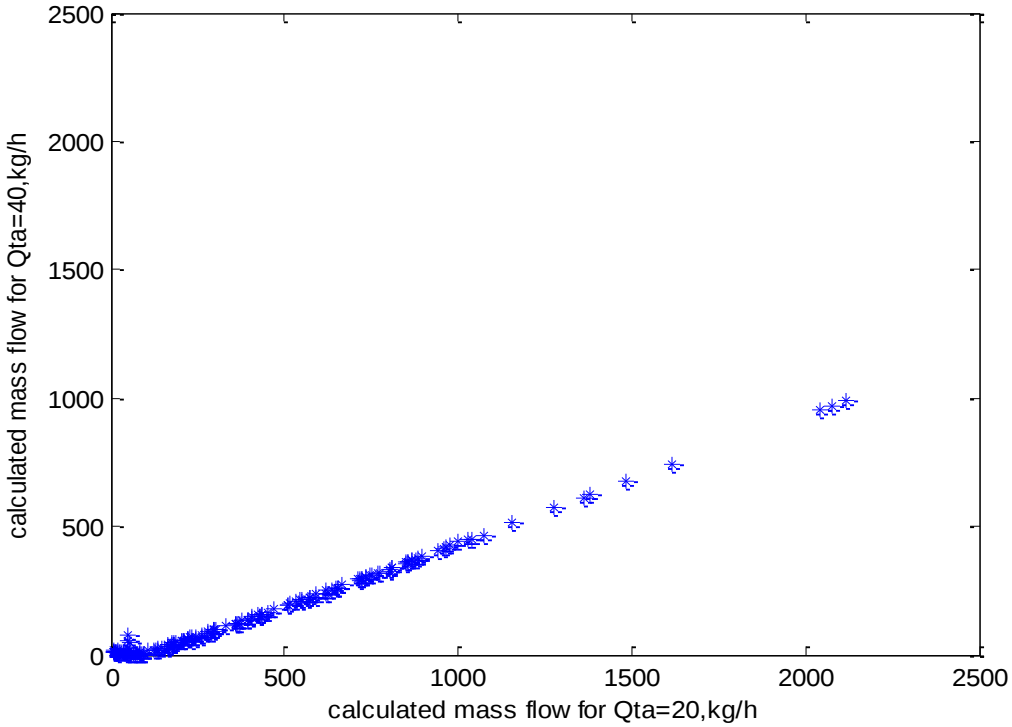

Figure 5-42: Calculated mass flow rate for different values of Qta

6 Conclusion

This report is a result of investigation of influence of geometrical features on capacity of industrial scale vertical air-lifters. The main aim of the present study was to investigate the influence of fluidization air flow rate $\dot{Q}_{FA}$, transport air flow rate $\dot{Q}_{TA}$, and nozzle position z on mass flow rate of solids in vertical air-lifters, by adopting a similar approach as proposed in Ratnayake (12). For this purpose the mathematical model for calculation of solids mass flow rate for vertical air-lifters was developed based on K-model for pneumatic conveying systems. In order to perform calculations for wide range of input data and to save the time, the mathematical model was programmed by using MatLab software. Calculations were done by two methods: based on instantaneous data for pressure drop coefficient K_{st} and based on average value of K_{st}. In addition, the calculations were performed for two types of conveyed material: zirconium oxide and glass beads. As the results show, the model simulation based on average value of pressure drop coefficient K_{st} gives a significant error and the model cannot be used for prediction of mass flow rate of solids for vertical air-lifters. Such conclusion can be made in case of both experiments with zirconium oxide and with glass beads. After consideration of the results of calculation based on instantaneous values of pressure drop coefficient K_{st} it can be concluded that developed model is suitable for calculation of mass flow rate of solids in vertical air-lifters regardless of the conveyed material. Model gives the best result based on online calculations of pressure drop coefficient but it also gives satisfactory results in case of using calculated K_{st} values for predicting of solids mass flow rate for different experimental conditions. After the evaluation of influence of operating conditions on solids mass flow rate in vertical air-lifters it can be concluded that the fluidization air flow rate $\dot{Q}_{FA}$ most affects the capacity. Transport air flow rate $\dot{Q}_{TA}$ also influences on mass flow rate of solids in vertical air-lifters. The nozzle position z has the least impact on capacity of vertical air-lifters. Results obtained in this study can be useful for predicting the solids mass flow rate in industrial scale vertical air-lifters and can be considered as a starting point for further research activities.

7 Suggestions for further work

As it was concluded the mathematical model can be applied for calculation of solids mass flow rate in vertical air-lifters based on instantaneous values of pressure drop coefficient K_{st}. However, the model has some uncertainties due to that fact that it was developed based on K-model which is used for calculation the parameters of pneumatic conveying systems. Moreover, the mathematical model uses experimental data as input variables for calculations. It may lead to uncertainties in results because of instrumentation error in experiment and electronic noise during the measuring of pressure changes in the transport pipe. As suggestions for further work, it can be considered to study different ways of avoiding model uncertainties. These uncertainties can be avoided by validation and calibration of model, filtering of measured data, calibration of measuring equipment.

References

1. **De Silva, Sunil R.** *Transport of particulate materials - Mechanical transport.* Porsgrunn, Norway : s.n., 1995.

2. **M, Sondalini.** [Online] [Cited: 02 05, 2013.] http://www.maintenanceresources.com/referencelibrary/ezine/beltcontuning.htm.

3. **G.J, Steele.** Bulk Solid Handling. [Online] september 28, 2009. [Cited: february 2, 2013.] http://www.bulk-solids-handling.com/conveying_transportation/pneumatic_conveying/articles/258627/.

4. **Klinzing G.E., Rizk F., Marcus R., Leung L.S.** *Pneumatic Conveying of Solids; A Theoretical and Practical Approach.* 2010.

5. **G.E., Klinzing.** University of Pittsburgh. [Online] [Cited: februar 3, 2013.] http://www.engineering.pitt.edu/Chemical/Documents/Historical_Review_of_Pneumatic_Conveying_and_Solids_Processing_World_Wide/.

6. *The Evolution of the Practice of Pneumatic Conveying.* **M.R., Hugget.** Jersey, Channel Islands : s.n., 1987. Pneumatech 3, Third International Conference on Pneumatic Conveying Technology.

7. **W.H., Link.** *Investigation of the Efficacy of the Flow Enhancer and the Indentification of the Beginning of the Unstable Zone in Pneumatic Conveying Systems.* Pittsburgh, USA : School of Engeneering, University of Pittsburgh, 1998.

8. **S.R., De Silva.** *Transport of particulate Materials: Dilute Phase Pneumatic Transport.* Porsgrunn, Norway : s.n., 1995.

9. **Mills D., Jones M.G., Agarwal V.K.** *Handbook of Pneumatic Conveying Engineering.* New York : Marcel Dekker,Inc., 2004.

10. Shinshin International, Inc. [Online] 2007. [Cited: february 4, 2013.] http://www.ssintl.co.kr/test/product_3_7.html.

11. H.V.Equipments Pvt. Ltd. [Online] [Cited: february 4, 2013.] http://hvepl.com/what-we-make.html.

12. **C., Ratnayake.** A Comprehensive Scaling Up Technique for Pneumatic Transport Systems. Porsgrunn, Norway : Department of Technology, Telemark University College, 2005.

13. **D., Geldart.** *Gas Fluidization Technology.* s.l. : Wiley, 1986.

14. **S.R., de Silva.** *Fluidization, De-aeration and their effect on systems selection and design.* Porsgrunn, Norway : Telemark Technological Centre, 1994.

15. **Wen C.Y., Yu Y.H.** *A Generalized Method for Predicting Minimum Fluidizing velocity.* s.l. : A.I.Chem.E.J., 1966.

16. **F.A., Zenz.** *Industrial Engineering Chemistry.* 1949.

17. **Zenz F.A., Othmer D.F.** *Fluidization and Fluid Particle Systems* . New York : Reinhold, 1960.

18. **Yousfi Y., Gau G.** *Chem. Eng. Sci.* 1974.

19. **C., Yang W.** *Proceedings Pneumotransport 3.* Cranfield, England : BHRA Fluid Engineering, 1977.

20. **Davidson J.F., Harrison D.** *Fluidized Particles.* Cambridge : Cambridge University Press, 1963.

21. **T.N, Smith.** *Chem.Eng.Sci.* 1978.

22. **Slis P.L., Willemse Th.W., Kramers H.** *Appl. Sci. Res.* 1959.

23. **Richardson J.F., Zaki W.N.** *Trans. Inst. Chem. Eng.* 1954.

24. **D., Mills.** *Pneumatic Conveying Design Guide.* Butterworth : s.n., 1990.

25. **Wypych P.W., Arnold P.C.** *On Improving Scale-up Procedures for pneumatic Conveying Design.* s.l. : Powder Technology, 1987.

26. **O., Molerus.** *Principles of flow in disperse systems.* s.l. : Chapman & Hall, 1993.

27. **Decamps F., Dumont G., Goossens W.** *Vertical pneumatic conveyor with a fluidized bed as mixing zone.* s.l. : Powder Technology, 1972.

28. **Leung L.S., Towler B.F.** *Design of vertical pneumatic conveyor with a fluidized bed as a mixing zone.* s.l. : Powder Technology, 1973.

29. **Chladek J., Enstad G.G., Melaaen M.C.** Effect of Operating Conditions and Particle Properties on Performance of Vertical Air-Lift. 2011 : Powder Technology.

30. **Mathiesen V., Solberg T.** Laser-based flow measurements of dilute vertical pneumatic transport. s.l. : Chem. Eng. Commun, 2004.

31. **Raczek J., Palica M.** *Selection of the gas working velocity in vertical pneumatic conveying systems for binary mixtures.* s.l. : Chem Eng Process, 1997.

32. *Scaling Pneumatic Conveying Characteristics for Pipeline Pressure.* **Keys S., Chambers A.J.** Oslo, Norway : s.n., 1993. International Symposium: Reliable Flow of Particulate Solids II.

Appendices

Appendix1. The example of MatLab code for model simulation. Script was used for calculating mass flow rate of solids in vertical air-lifter for experiment with glass beads at the following experimental conditions:

$$\dot{Q}_{FA} = 100\ {}^{m^3}/_{h},\ \ \dot{Q}_{TA} = 40\ {}^{m^3}/_{h},\ \ z = 3\ cm$$

```
%  Vertical air lifter

clear all

% import data from excel

filename='Calculations.xlsx'; % excel file with data
sheet=5; %the list in Excel file from which the first data set is imported
sheet1=7; %the list in Excel file from which the new data set is imported

xlRange='G6:G167';
xlRange1='H6:H167';
xlRange2='C6:C167';

xlRange3='H6:H167';
xlRange4='G6:G167';
xlRange5='C6:C167';
ms=xlsread(filename,sheet,xlRange); % meassured mass flow rate for the first data set
ms_new=xlsread(filename,sheet1,xlRange4);% meassured mass flow rate for new data set
delta=xlsread(filename,sheet,xlRange1); % measured pressure difference for the first data set
delta_new=xlsread(filename,sheet1,xlRange3);% measured pressure difference for new data set
t=xlsread(filename,sheet,xlRange2); % time intervals for the first data set
t_new=xlsread(filename,sheet1,xlRange5); % time intervals for the new data set

% constant variables

h=4; %height of air-lifter
%z=0.02; %nozzle position, m
z1=0.03; % nozzle position, m
Qta=20; %volume flow rate of transport air
Qta1=40; % volume flow rate of transport air
Qfa=100; %volume flow rate of fluidization air
%Qfa1=500; % volume flow rate of fluidization air
ro_a=1.2041; % density of air
%dp=0.26; % particle diameter for zirconium oxide, mm
dp=0.15; % particle diameter for glass beads, mm
D=0.042; % diameter of the transport pipe, m

% space for storing calculated data

delta_p=zeros(size (delta));
delta_p_new=zeros(size(delta_new));
ro_sus=zeros(size(delta));
Kst=zeros(size(delta));
m_s=zeros(size(delta));
m_s1=zeros(size(delta));
```

```
% for – loop for calculating mass flow rate

        for i=1:size(delta)

          delta_p(i)=delta(i)*1000; % pressure drop in bar
          delta_p_new(i)=delta_new(i)*1000;% pressure drop for new data set
          ro_sus(i)=(ro_a*Qfa+ms(i))/Qfa;% suspention density
          %ro_sus_new(i)=(ro_a*Qfa+ms_new(i))/Qfa;% suspention density for new data set
          Kst(i)=delta_p(i)./(8*ro_sus(i).*(Qta^2)/(3.14^2*D^4)) % pressure drop coefficient
          %Kst(i)=delta_p_new(i)./(8*ro_sus_new(i).*(Qta^2)/(3.14^2*D^4)); % pressure drop coefficient
          for new data set
          %Kst_aver=mean(Kst);%average value of Kst
          %Kst1(i)=8.4537*10^(-6);

          m_s(i)=abs((ro_a*Qfa-Qta*(delta_p(i)*(3.14^2)*(dp^4)*D)/(8*Kst(i)*(Qta^2)*(h+z1)))/((delta_p(i)
                  *(3.14^2)*(dp^4)*D)/((8*Kst(i)*(Qta^2)*ro_a*(h+z1))-1))); % mass flow rate of solids

          m_s1(i)=abs((ro_a*Qfa-Qta1*(delta_p_new(i)*(3.14^2)*(dp^4)*D)/(8*Kst(i)*(Qta1^2)*(h+z1)))/
                  ((delta_p_new(i)*(3.14^2)*(dp^4)*D)/((8*Kst(i)*(Qta1^2)*ro_a*(h+z1))-1))); %mass flow
                  rate of solids for the new data set
          i=i+1;
        end

% plotting the results

figure
plot (t,Kst,'r')
hold on
%plot(t,Kst1,'*')
%axis([0 120 0 1.8*10^(-5)])
%plot(t_new,Kst,'m') % plot Kst calculated based on new data set
xlabel('time,s')
ylabel('Kst')
%legend('Kst','average Kst')
title('pressure drop coefficient')

figure
plot(t,ms,'g')
hold on
plot(t,m_s,'m')
xlabel('time,s')
ylabel('ms, kg/h')
legend('measured mass flow rate, kg/h','calculated mass flow rate, kg/h')
figure
plot(ms,m_s,'b*')
%axis([0 600 0 600])
% xlabel('measured mass flow for Qfa=600,kg/h')
% ylabel('calculated mass flow for Qfa=600,kg/h')

xlabel('measured mass flow for Qta=20,kg/h')
ylabel('calculated mass flow for Qta=20,kg/h')

figure
plot(t_new,ms_new,'g')

hold on
plot(t_new,m_s1,'b')
%axis([0 120 0 1800])
xlabel('time,s');
ylabel('ms,kg/h');
```

```
% legend('meassured mass flow rate for Qfa=100, kg/h','calculated mass flow rate for Qfa=100, kg/h')

 legend('meassured mass flow rate for Qta=40, kg/h','calculated mass flow rate for Qta=40, kg/h')
title('calculated vs.meassured mass flow rate of solids, kg/h')

figure
plot(ms_new,m_s1,'g*')
axis([0 10000 0 10000])
% xlabel('measured mass flow for Qfa=100,kg/h')
% ylabel('calculated mass flow for Qfa=100,kg/h')

xlabel('measured mass flow for Qta=40,kg/h')
ylabel('calculated mass flow for Qta=40,kg/h')

figure
plot (m_s, m_s1,'*')
axis([0 2500 0 2500])
% xlabel('calculated mass flow for Qa=600,kg/h')
% ylabel('calculated mass flow for Qfa=100,kg/h')

xlabel('calculated mass flow for Qta=20,kg/h')
ylabel('calculated mass flow for Qta=40,kg/h')
```